AD-A046 150   SOLAREX CORP ROCKVILLE MD   F/G 10/2

NONREFLECTING VERTICAL JUNCTION SILICON SOLAR CELL OPTIMIZATION--ETC(U)

JUL 77 J WOHLGEMUTH, J LINDMAYER, A SCHEININE F33615-76-C-2058

UNCLASSIFIED   AFAPL-TR-77-38   NL

| OF |

AD A046150

END

DATE FILMED

12-77

DDC

AD A046150

AFAPL-TR-77-38

(12)

NONREFLECTING VERTICAL JUNCTION SILICON SOLAR CELL OPTIMIZATION

SOLAREX CORPORATION
1335 PICCARD DRIVE
ROCKVILLE, MARYLAND 20850

JULY 1977

TECHNICAL REPORT AFAPL-TR-77-38
Interim Report for Period April 1976 – April 1977

Approved for public release; distribution unlimited.

AIR FORCE AERO PROPULSION LABORATORY
AIR FORCE WRIGHT AERONAUTICAL LABORATORIES
AIR FORCE SYSTEMS COMMAND
WRIGHT-PATTERSON AIR FORCE BASE, OHIO 45433

NOTICE

When Government drawings, specifications, or other data are used for any purpose other than in connection with a definitely related Government procurement operation, the United States Government thereby incurs no responsibility nor any obligation whatsoever; and the fact that the government may have formulated, furnished, or in any way supplied the said drawings, specifications, or other data, is not to be regarded by implication or otherwise as in any manner licensing the holder or any other person or corporation, or conveying any rights or permission to manufacture, use, or sell any patented invention that may in any way be related thereto.

This final report was submitted by Solarex Corporation, under Contract F33615-75-C-2058. The effort was sponsored by the Air Force Aero Propulsion Laboratory, Air Force Systems Command, Wright-Patterson AFB, Ohio under Project 3145, Task 314519 and Work Unit 31451959 with Dr. W. Patrick Rahilly (AFAPL/POE-2) as Project Engineer. Dr. John Wohlgemuth of Solarex Corporation was technically responsible for the work.

This report has been reviewed by the Information Office (ASD/OIP) and is releasable to the National Technical Information Service (NTIS). At NTIS, it will be available to the general public, including foreign nations.

This technical report has been reviewed and is approved for publication.

W. Patrick Rahilly

Project Engineer

FOR THE COMMANDER

Joseph Wise

Technical Area Manager

"If your address has changed, if you wish to be removed from our mailing list, or if the addressee is no longer employed by your organization please notify AFAPL/POE-2 ***,W-P AFB, OH 45433 to help us maintain a current mailing list".***

Copies of this report should not be returned unless return is required by security considerations, contractual obligations, or notice on a specific document.

AIR FORCE/56780/25 October 1977 — 225

UNCLASSIFIED

SECURITY CLASSIFICATION OF THIS PAGE (When Data Entered)

19 REPORT DOCUMENTATION PAGE		READ INSTRUCTIONS BEFORE COMPLETING FORM
18 1. REPORT NUMBER AFAPL-TR-77-38	2. GOVT ACCESSION NO.	3. RECIPIENT'S CATALOG NUMBER
6 4. TITLE (and Subtitle) NONREFLECTING VERTICAL JUNCTION SILICON SOLAR CELL OPTIMIZATION.		5. TYPE OF REPORT & PERIOD COVERED 15 May 76 - 15 May 77
		6. PERFORMING ORG. REPORT NUMBER
10 7. AUTHOR(s) John ~~J.~~ Wohlgemuth, J. Lindmayer, A. Scheinine		8. CONTRACT OR GRANT NUMBER(s) 15 F33615-76-C-2058 new
9. PERFORMING ORGANIZATION NAME AND ADDRESS Solarex Corporation 1335 Piccard Drive Rockville, MD 20850		10. PROGRAM ELEMENT, PROJECT, TASK AREA & WORK UNIT NUMBERS 11 Jul 77 12 82p.
11. CONTROLLING OFFICE NAME AND ADDRESS Department of the Air Force Air Force Aero Propulsion Laboratory Wright-Patterson Air Force Base, OH 45433		12. REPORT DATE August 1977
		13. NUMBER OF PAGES
14. MONITORING AGENCY NAME & ADDRESS(if different from Controlling Office) 16 3145 17 19		15. SECURITY CLASS. (of this report) UNCLASSIFIED
		15a. DECLASSIFICATION/DOWNGRADING SCHEDULE

16. DISTRIBUTION STATEMENT (of this Report)

"Approved for public release; distribution unlimited"

17. DISTRIBUTION STATEMENT (of the abstract entered in Block 20, if different from Report)

9 Interim rept. May 76 - May 77,

18. SUPPLEMENTARY NOTES

19. KEY WORDS (Continue on reverse side if necessary and identify by block number)

Vertical Junction Solar Cells
Silicon Solar Cells
Solar Cells
Space Photovoltaic Power

62203F

20. ABSTRACT (Continue on reverse side if necessary and identify by block number)

This work on nonreflective vertical-junction silicon solar cells has resulted in high conversion efficiency radiation resistant solar cells. New techniques of oxidation growth and the use of photolithography enable the use of an orientation dependent etch to produce grooves 5-10 microns wide and over 100 microns deep. These silicon wafers have been processed into solar cells with all of the processes performed at temperatures compatible with

DD FORM 1 JAN 73 1473 EDITION OF 1 NOV 65 IS OBSOLETE

Unclassified

SECURITY CLASSIFICATION OF THIS PAGE (When Data Entered)

392 910

mt

producing high efficiency solar cells. A theoretical calculation of the generated current for the vertical junction structure was performed. It indicates the decreased dependence on carrier diffusion length and, therefore, the reduced effect of radiation damage on collection efficiency for vertical junction solar cells. Vertical junction solar cells 2 cm x 2 cm in size have been fabricated with AMO conversion efficiencies greater than 13%. These cells have shown superior radiation resistance.

ACCESSION for	
NTIS	White Section ☑
DDC	Buff Section ☐
UNANNOUNCED	☐
JUSTIFICATION	
BY	
DISTRIBUTION/AVAILABILITY CODES	
	CIAL
A	

TABLE OF CONTENTS

LIST OF ILLUSTRATIONS

LIST OF TABLES

SECTION I
INTRODUCTION

During the first year of this research program at Solarex, the vertical junction silicon solar cell has progressed from a theoretical possibility to a practical reality. For the first time, solar cells have been fabricated which exhibit both high efficiency and radiation resistance. The vertical junction cell makes many new space applications feasible.

Silicon solar cells have been used for years as a primary energy source for space applications. The availability of continuous, relatively high density solar energy makes solar cells ideal for space use. It has been found, however, that the output of the solar cells degrades with time, due to radiation damage. In many space environments there is a high level of radiation leading to severe degradation of solar cells placed in these environments. A radiation resistant solar cell would prolong the lifetime of the mission, enable planners to reduce the initial weight of the solar array, and allow the placement of experiments in certain orbits now prohibited. For long-term application, a radiation resistant solar cell is a necessity.

Vertical junction solar cells were initially proposed by J. F. Wise (Ref. 1) to alleviate the degradation of solar cells in space due to radiation damage. Theoretical analysis of the vertical junction cell by Rahilly (Ref. 2), Stella and Gover (Ref. 3), and Chadda and Wolf (Ref. 4) predicted that the vertical junction solar cell theoretically can be a high efficiency radiation resistant cell. Because of the inherent advantage of the vertical junction geometry, experimental attempts at fabrication were begun by Smeltzer, et al (Ref. 5), and Lloyd et al (Ref. 6 and Ref. 7) at Texas Instrument Corporation under contract to AFAPL. This initial experimental program resulted in the fabrication of vertical junction cells with indications of improved radiation resistance. However, the efficiencies of these cells were too low for them to be useful for actual applications.

In the past year, a research program at Solarex Corporation has resulted in the fabrication of vertical junction solar cells with dramatically higher efficiencies. For 2 x 2 cm vertical junction solar cells, efficiencies of greater than 13% AMO have been obtained. As expected, the radiation resistance of these cells is far superior to planar cells. With these cells it is now possible to design space missions where high level radiation exposure is expected. Also, with these cells the size of the solar array can be reduced and still retain an adequate end-of-life-power performance.

The vertical junction solar cell consists of deep grooves etched into the silicon surface. The grooves are etched close together (on the order of 15 microns between centers) so that only the walls (on the order of 5 to 10 microns thick) are left between the grooves. The solar cell junction follows the surface up and down the walls. Figure 1 is a diagram of such a geometry. Since the walls are so narrow, carriers generated in the walls, say by incident light, are already close to a collecting junction. Therefore, even if the cell is exposed to radiation causing a decrease in the diffusion length (a measure of the distance the carriers can move without recombining), the carriers in the walls will still be able to transverse the short distance to the junction and be collected. In a planar cell, many carriers must travel from deep in the bulk

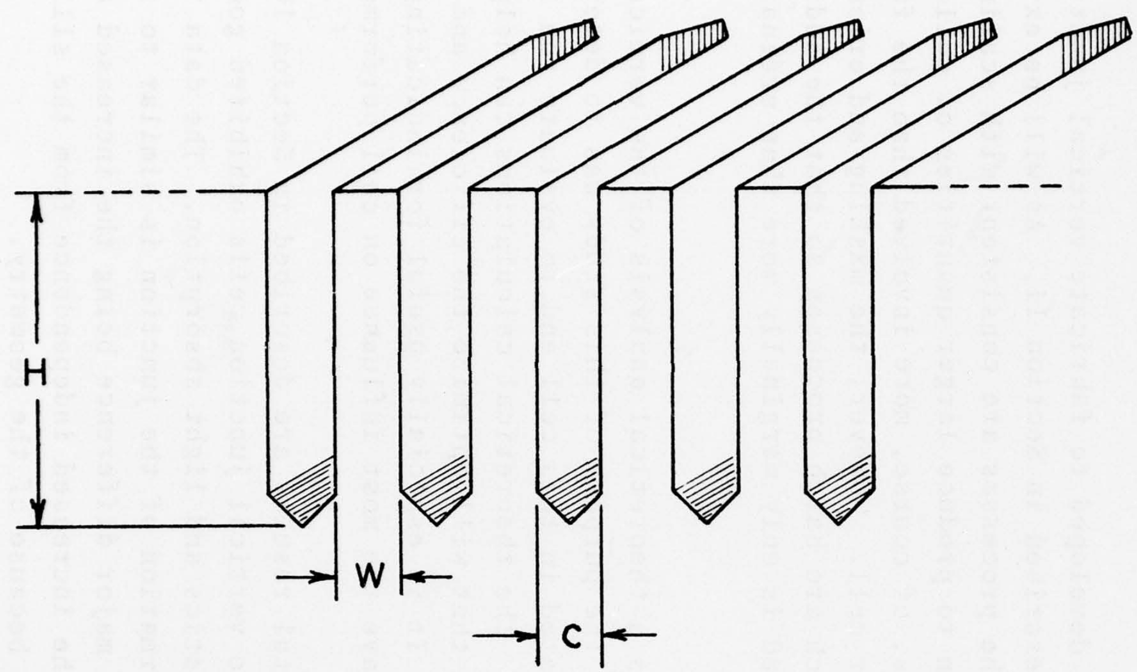

Figure 1: Structure of Vertical Junction Solar Cell

all the way to the junction. Then, upon irradiation, the increase in defect density decreases the carrier lifetime so much that they never reach the junction. In the vertical junction, most of the carriers are generated in the walls where the lifetime will still be long enough for the carriers to be collected.

The processes developed to fabricate vertical junction solar cells are described in Section II. As will be explained, all of the processes are consistent with scaling up of the fabrication to produce larger quantities of cells. The fabrication is, of course, more involved than the fabrication of a planar cell. However, the masking and orientation dependent etch are batch processes so that the additional processing involved is only marginally more than ordinary pyramid cells.

Section III is a theoretical analysis of the vertical junction solar cell. The purpose of this study was to determine the current generated in this cell and to evaluate the radiation degradation. The theoretical calculations can help us choose geometries that will optimize the efficiency and radiation resistance. It is especially useful for indicating the parameters that have the most influence on cell performance.

The experimental results are described in Section IV. As will be shown, the vertical junction cells exhibited good electrical characteristics and light absorption. The data indicated that the formation of the junction is similar to that of planar cells, the major difference being the increased area and, of course, the increased independence from the silicon material lifetime because of the geometry.

The final section summarizes the advancements made in vertical junction solar cells technology to date. There is also a discussion of the plans for the remainder of the contract in order to realize the goal of 15% efficient vertical junction solar cells.

SECTION II
EXPERIMENTAL PROCEDURES

The initial work on vertical junction solar cells concentrated on developing experimental processing procedures that would produce high efficiency solar cells. This meant that no processes could be employed that would require placing the silicon in an environment with a temperture much greater than 900°C. For the initial work, some of the processes developed during previous work on vertical junction cells were used. However, as work progressed, changes were made to improve the processes, especially to reduce the time and effort required to fabricate the cells without reducing the efficiency of the cells. The sections below describe the process steps used and explain how and why changes in procedure were implemented.

1. Silicon Material

During the orientation dependent etch, the 111 plane etches at a much slower rate than the other silicon planes. Therefore, the silicon wafer should have 111 planes normal to the surface so that deep grooves can be etched leaving vertical 111 walls. The surface of the proper silicon wafers for this application are oriented on the 110 plane. While 110 silicon ingots can be grown, they are extremely expensive and cannot be obtained dislocation free. The most convenient source of dislocation free 110 wafers is from 111 ingots aligned and cut perpendicular to the 111 axis leaving 110 wafers. To facilitate alignment of the etching mask to the 111 planes, the 110 slices can be x-ray oriented and a flat cut on the 111 plane.

Since fine line photolithography is performed on the silicon wafers, the surface must be smooth. All of the silicon used to date has been chem-mech polished with cupric nitrate solution as developed by Mendel and Yang (Ref. 8).

2. Oxide Growth for Masking the Etch

To etch grooves into silicon, an effective alkaline etchant mask is required. Thermally grown silicon dioxide can be used as such a mask, but it is slowly dissolved by the etchant. Therefore, it is necessary to use a layer of oxide several thousand Angstroms thick in order to etch deep grooves. Normal thermal oxidation will not produce such thick layers of oxide at temperatures low enough to be compatible with the fabrication of high efficiency solar cells.

As is well known, phosphosilicate glasses form readily during solar cell diffusions. This oxide alone, however, is not sufficient to serve as the etchant mask, since it is neither thick enough nor etch resistant enough. However, combining the diffusion growth with an oxide growth in steam (which is also known to speed oxide growth) results in adequate oxide masks. The silicon slices were diffused with phosphorus at temperatures between 800°C and 860°C for several minutes to grow a thin layer of phosphosilicate glass. Then the slices are steamed at the same temperature, resulting in the growth of an oxide of the required thickness.

3. Orientation and Placement of the Groove Pattern

Standard photolithography techniques are employed to place the pattern on the silicon. Lines 5 microns wide must be repeatedly placed across the whole surface. Because of this fine geometry, care must be taken to have a clean silicon oxide surface and to remove any impurities from the photoresist itself.

The photolithography pattern must be aligned very accurately to the 111 plane so the etch will produce deep, narrow grooves. Originally, a fan pattern with finger separated by .2° was aligned to the x-ray oriented flat. The fan pattern was orientationally dependent etched to determine the optimal alignment to the 111 plane. The photomask groove pattern was then optically aligned to the narrowest etched groove in the fan pattern. While the method works, it requires an extra orientation dependent etch and either a thicker original oxide or the growth of two oxides to withstand the two orientation dependent etches that are performed. This technique also required a great deal of time analyzing the etch fan pattern and then aligning the mask grooves to the chosen fan pattern line.

To simplify the procedure, an attempt was made to optically align the mask directly to the x-ray oriented flat. It was found that this process resulted in an orientation dependent etch indistinguishable from that obtained from the fan pattern alignment. Therefore, to save process time, the initial orientational dependent fan pattern etch has been eliminated from the procedure.

Recently, the masks have had flat stops optically aligned to the groove pattern and permanently mounted to them. Then the flat on the cell is mechanically placed against the flat on the mask for photolithography exposure. The pattern seems to be aligned as well as those aligned by the previous technique.

4. Oxide Etch

The photoresist on the surface now acts as a mask for the oxide etch. The etchant is $6NH_4F$:1 HF. The etchant does not attack the photoresist or the silicon but does remove all of the oxide. Several minutes of etching removes the oxide from the windows with a minimum of undercutting.

5. Orientational Dependent Etch

The orientational dependent etch of silicon in KOH has been studied in detail by Kendall (Ref. 9). Etch rate differences of 400 to 1 have been obtained. While the largest rate difference would lead to the deepest groove depths at the same width, there are other considerations in choosing a particular etchant. Since the oxide does slowly dissolve in KOH solution, it is necessary to use an etchant that does not etch away the oxide mask before reaching the required groove depth. It would also be desirable to have an etchant that does not require an excessive amount of time to form the grooves.

The etchant found to satisfy best the criteria is 30% KOH in H_2O at 70° to 75°C. With this etchant, grooves 4 mils deep are etched within one hour with the original groove mask width of 5 microns increasing to 7 microns. The walls are extremely straight and parallel except near the tops where an isotropic rounding etch has changed the shape. This expansion of the grooves may be due to slight misalignment of the mask with the 111 plane or undercutting of the oxide mask during the oxide etch.

Figure 2 is a scanning electron microscope picture at a magnification of 250 of a vertical junction cell broken per-

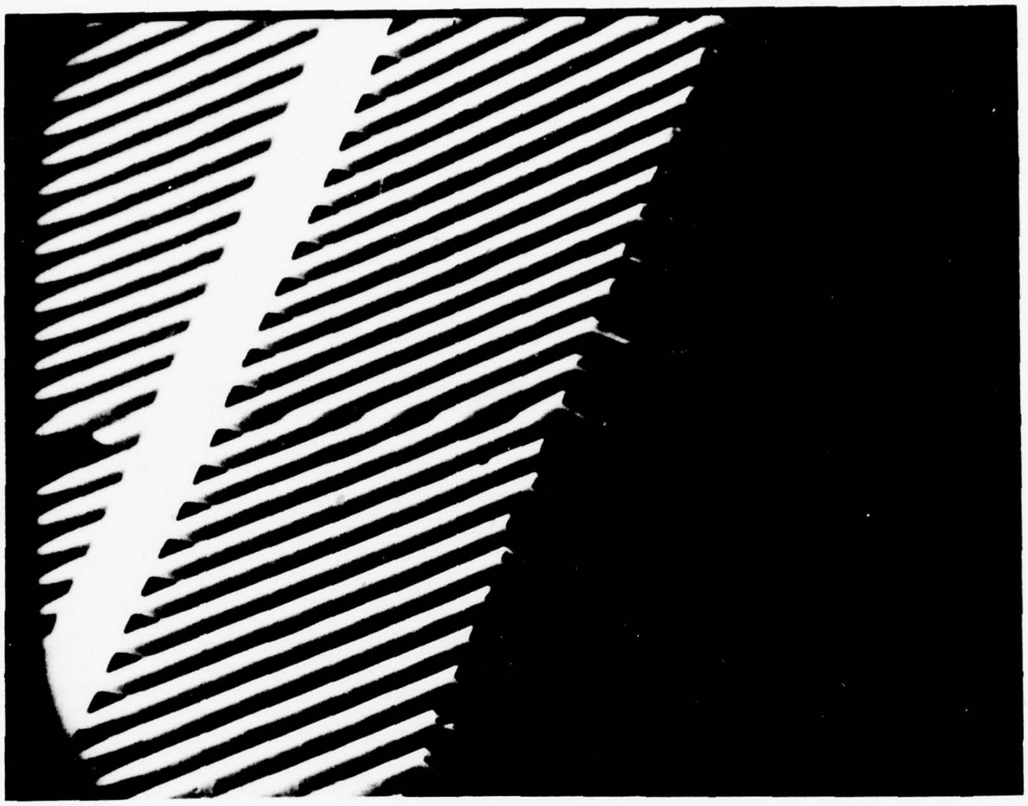

Figure 2: Scanning Electron Microscope Picture at a Magnification of 250 of a Vertical Junction Solar Cell Broken Perpendicular to the Grooves.

pendicular to the grooves. Figure 3 is an SEM picture at 500x of the broken edge of a vertical junction cell at a different angle than Figure 2. Notice the uniformity of depth and the straightness of the walls except near the top where they are rounded on purpose. Figure 4 is an SEM picture at 100x looking perpendicular to the grooves along the edge of the broken buss bar. Note the slant of the 111 plane as it slopes toward the bottom of the groove. This shows the strength of the buss bar ribs and indicates why the cells are not overly susceptible to breakage. Figure 5 is an SEM picture at 3000x of the beginning of a groove. Every exposed plane inside the groove is a 111 plane. The elongation of the groove during etching is very small.

While the etch is usually performed on well-aligned wafers resulting in cells as shown in Figures 2-5, sometimes the 111 plane is not well aligned to the groove pattern. In this case, the grooves etch wider, resulting in very narrow walls. Figure 6 is an SEM picture at 500x perpendicular to some very narrow walls. Figure 7 is a SEM picture at 2000x looking down on these walls. Note the misalignment ridges running across the grooves. These ridges are the change from one 111 plane to another and indicate how misaligned the pattern originally was. These thin walls are extremely fragile, but we were still able to make functional solar cells out of some of the wafers etched like this.

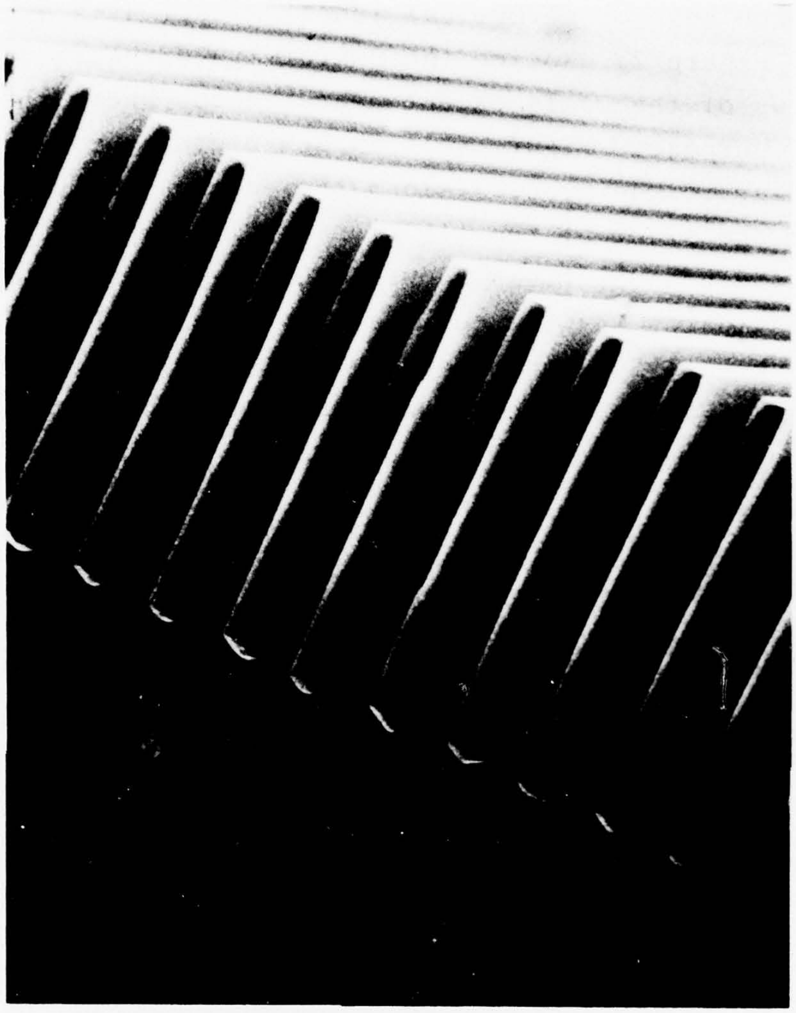

Figure 3: An SEM Picture at 500x of a Vertical Junction Cell Broken Perpendicular to the Grooves.

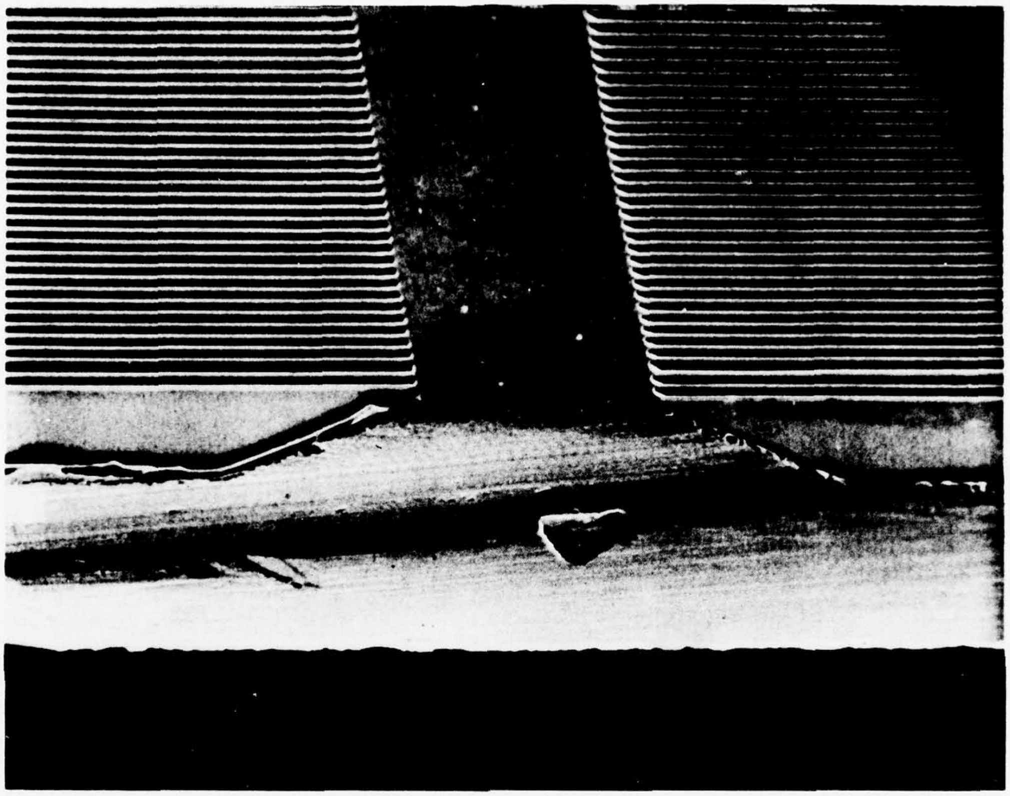

Figure 4: An SEM Picture at 100x Looking Perpendicular to the Groove Along the Edge of a Broken Buss Bar.

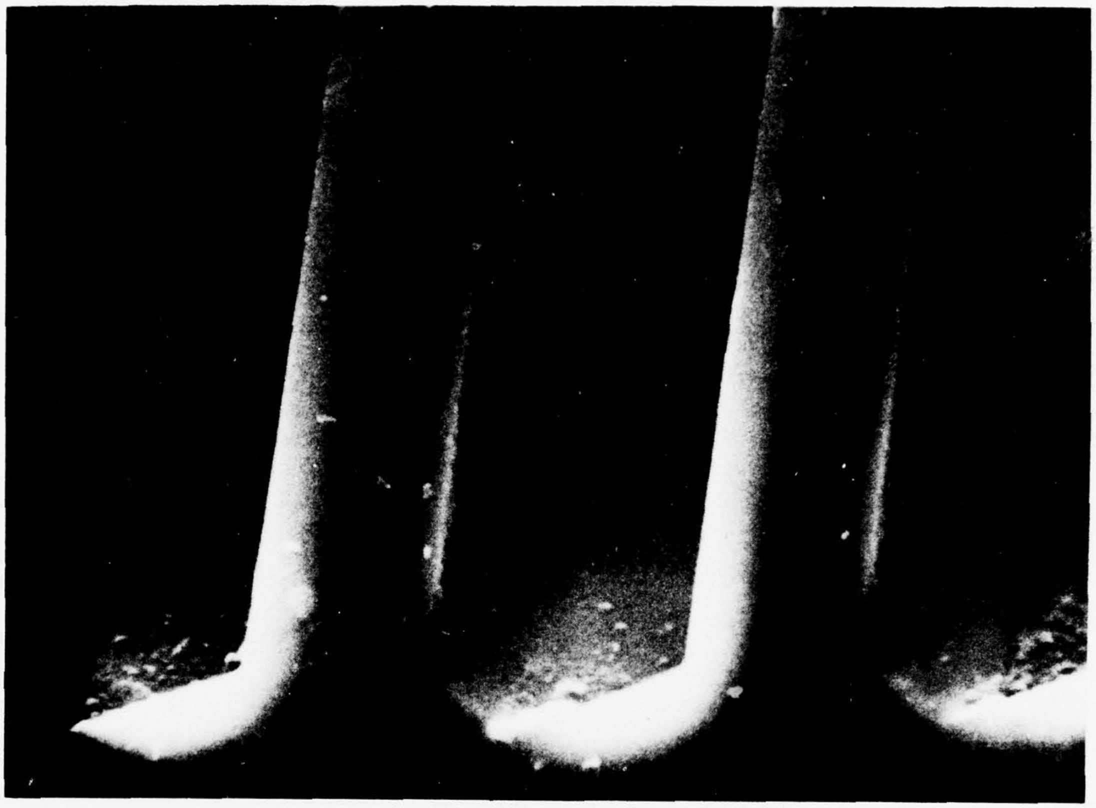

Figure 5: An SEM Picture at 3000x of the Start of the Grooves.

Figure 6: An SEM Picture at 500x of Narrow Etched Walls.

Figure 7: An SEM Picture at 2000x of the Same Narrow Walls as Figure 6 at a Different Angle.

6. Oxide Removal and Shaping Etch

After the orientation dependent etch, the remainder of the oxide is removed by a second etch in HF solution in H_2O. Once again, this etch is used so that there is no damage done to the silicon.

During the oxide growth, phosphorous was diffused into the silicon. This phosphorous still remains in the top of the walls. To maximize the light absorption by the cell, it would be advantageous to shape the tops of the walls. Therefore, an isotropic etch must be performed to remove the phosphorous and to shape the wall tops. Both alkaline and acid etches have been used for this purpose. The alkaline etches tend to produce very pointed and jagged walls with many crystal planes exposed. While this type of wall does aid in total optical absorption, it results in very fragile walls and because of the many crystal planes exposed can lead to deterioration of the fill factor. The acid etch used is a 1:3:8 (by volume) mixture of 49% HF, 70% HNO_3 and 98% CH_3COOH. A long etch (minutes) in this acid will also produce pointed tops. However, a short etch results in rounded walls, which are both strong and nearly non-reflecting. This type of etch has been employed on most of the cells and results in a satisfactory geometry.

7. Diffusion

Phosphine gas was used as the source of the phosphorous during diffusion. Diffusion temperatures between 840° and 913°C have been employed (see Section IV for a profile of the electrical properties as a function of diffusion temperature). The diffusion parameters such as flow rate, duration of treatment, and geometry during the process must be maximized for the vertical junction cell. The presence of multiple crystal planes as well as the need to diffuse down narrow grooves are special features of the vertical junction cell. However, the differences in diffusion process from planar to vertical junction cells are not major, and in reality the diffusion procedure is quite similar to that developed for planar cells.

8. Back Contacts

The formation of the back contact for vertical junction cells can be identical to that for planar cells. Our cells have been fabricated with a vacuum deposited and then alloyed aluminum p^+ back. On top of this, we have vacuum evaporated Ti-Pd and then covered this with Ag. The vertical junction cell requires no special back treatment and so could take advantage of any back contact development for planar cells.

9. Front Contact Metallization

Because of the steep walls, liquid photoresist cannot be used as a mask for placing the front contacts on the cells. All of the cells to date have had Ti-Pd metal contacts vacuum deposited using shadow masks and then covered with silver.

Originally the cells were aligned optically in the mask holder until the lines in the mask matched up with the buss bars on the cells. This is a slow, tedious procedure prone to human error. A new mechanical alignment system has been developed so that the cells are locked into place and, when the shadow mask is placed on top, it is automatically aligned in the correct position. An added advantage of this system is that the masks can be made inexpensively in house.

10. Anti-Reflective Coating

The anti-reflective coating used on all of the cells is Ta_2O_5 vacuum deposited by electron beam. The thickness deposited is the same as for planar cells. The AR coating is only effective on the planar area, such as the top of the walls. The AR coatings on vertical junction cells usually increase the efficiency by about 1%, while on the planar cells the increase is on the order of 20%. This in itself shows the non-reflective nature of the vertical junction cell.

11. Cover Slide

Cerium doped glass cover slides have been placed on vertical junction cells employing conventional Dow Corning Sylgard silicon adhesive. Attention to outgassing of the channels through the liquid silicon before cover attachment appears quite successful in removing air from the channels.

12. Geometry of Cells Fabricated

To test the procedures for fabricating vertical junction solar cells, the initial cells were fabricated with 50 micron grooves and 50 micron walls. While these cells are not fine enough geometry to be radiation resistant, this intermediate geometry enabled the initial procesing steps to be developed.

The actual radiation resistant vertical junction cells have geometries as shown in Figure 1, with initial groove widths of 5 microns with 10 microns between grooves. One buss bar and groove pattern used for most of the cells is shown in Figure 8. The grooves are 122 mils long. The buss

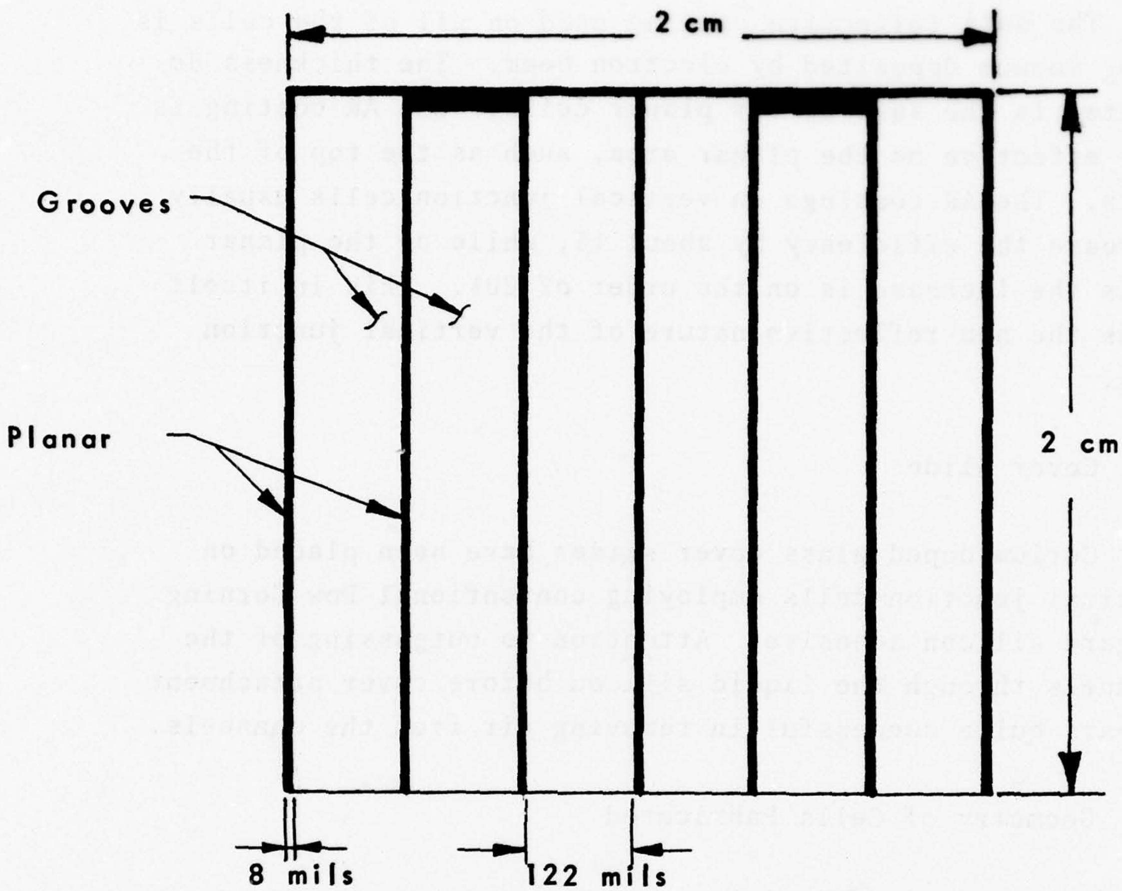

Figure 8: Diagram of the 7 Buss Bar Geometry Cell. Grooves Run Perpendicular to the 7 Busses.

bars are 8 mils wide. Initially, 4 mils of metallization were placed on each buss bar. Due to problems with contacts on the outer buss bars, later cells had 6 mils of metallization on the inner 5 busses with no metallization on the outer 2 busses. Some cells were fabricated with the geometry as shown in Figure 9. This pattern has an 8 mil buss bar centered between the busses from the pattern shown in Figure 8. Therefore, the inter-buss distance is 57 mils.

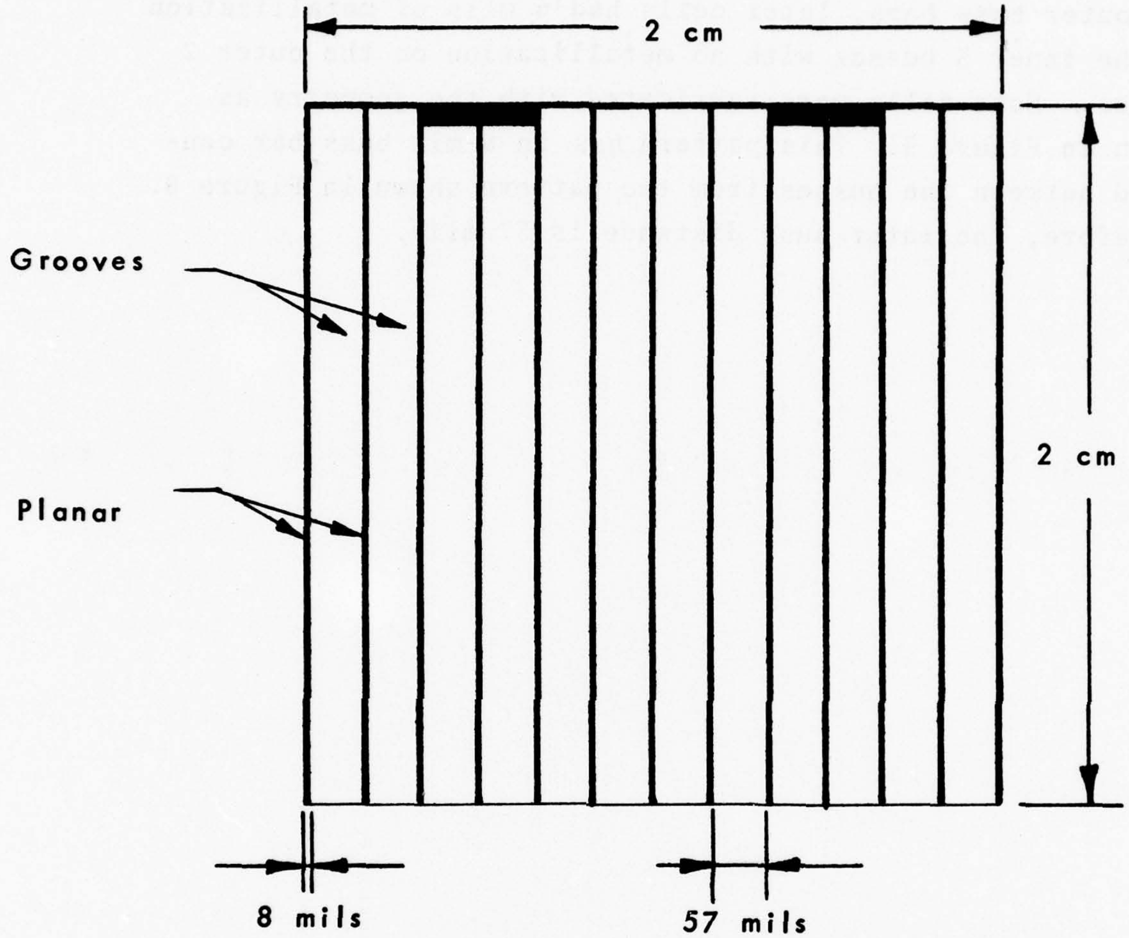

Figure 9: Diagram of the 13 Buss Bar Geometry Cell. Grooves Run Perpendicular to the 13 Busses.

SECTION III
THEORETICAL ANALYSIS

Since silicon has an indirect bandgap, photons with energy above but near the bandgap will travel far into the crystal before generating carriers. If the diffusion length is shortened due to radiation damage, then carriers generated far-meaning more than a diffusion length-from a junction will recombine before reaching the junction, and the output will decline. By etching multiple vertical junctions in a cell, more carriers are generated near a junction than is the case for a planar cell. This effect of junction geometry on carrier collection efficiency is evaluated quantitatively in the following pages, and the short circuit current and open circuit voltage of a VMJ is calculated and compared to a planar cell.

For a simple geometry, the short circuit current, which depends on where carriers are generated and how many make it to the junction, can be described with a single mathematical formula. This formula is a function of the absorption depth as well as the minority carrier diffusion length. In the following section, formulas are developed for the short circuit current for a planar solar cell with a junction on the front surface and for a vertical wall illuminated from 1) the plane facing into the groove, and 2) the top edge.

In the third section, it is shown how the solutions to these formulas can be used to predict the short circuit current of a vertical multijunction cell as a function of diffusion length when the effect of surface reflection is included. Also calculated is the open circuit voltage as

1) junction area is increased to create vertical junctions, and 2) as the diffusion length shortens.

The fourth section summarizes several studies of the minority carrier diffusion length as a function of damaging radiation.

1. Carrier Collection for Basic Geometries

A VMJ can be described as vertical walls on a horizontal substrate with a junction over all the surfaces. At the current density induced by AMO illumination, there is negligible voltage drop in the bulk* so that the total current can be described as the sum of several current sources without interaction between the sources. The current can be partitioned into sources due to light entering the top of the vertical walls, light entering the grooves and absorbed in the side of the walls, and light entering the horizontal substrate through the groove bottom. To find the current due to these three light paths, two geometries need to be analyzed: first, a planar junction for application to light entering the substrate below the grooves and for light entering the top of a vertical wall with a junction on the flat top, and, second, parallel junctions on a vertical wall for light entering the top and for light entering the side of the wall.

*To show that the current density is so low as to avoid interaction, majority carriers will first be considered, then minority carriers. Suppose the worst case voltage drop, namely the maximum possible AMO current of 51 ma/cm^2 moving through the entire cell thickness (250 microns) from front to back of a planar cell. A resistivity of one ohm-cm implies a voltage drop of 1.3 mV. The grooved region has about half as much silicon, hence, about twice the resistance. Still, only a few millivolts will appear across the entire bulk.

The distribution of minority carriers within a planar slice of silicon uniformly illuminated on one side is governed by the following formula.

$$L_n^2 \frac{d^2n}{dx^2} - n = \frac{-L_n^2 * a * H * \exp(-ax)}{D_n}$$

where H = number of photons entering silicon plane

a = light absorption coefficient

x = distance from front surface

L_n = minority carrier diffusion length

n = minority carrier density

D_n = minority carrier diffusion rate

The solution to this equation is

$$n = \frac{-H * a * \exp(-ax)}{D_n\{a^2 - (L_n)^{-2}\}} + K_1 \exp(x/L_n) + K_2 \exp(-x/L_n)$$

The boundary conditions are that the density of minority carriers at the front surface is zero because they are collected by a junction at the front surface under short circuit condi-

---

*(cont.) We must also show that the density of minority carriers remains significantly below the doping level. Using a photon flux of .3 x $10^{18}/cm^2$ sec. for AMO illumination, we can write an equation for diffusion current.

$$.3 \times 10^{18}/cm^2/sec = D_n \frac{dn}{dx}$$

where D_n = 10 cm^2/sec for 1 ohm-cm silicon

n = the density of electrons in the p-type bulk.

tions, and the back surface has a recombination velocity, S_n, which implies

$$n(x=0) = 0$$

$$D_n \left.\frac{dn}{dx}\right|_{x=B} = -S_n * n\ (x=B)$$

These boundary conditions yield values for K_1 and K_2 shown below.

$$K_1 = \frac{C_1 (1-C_2/C_4)}{(C_3/C_4 -1)}$$

$$K_2 = \frac{C_1(1-C_2/C_3)}{(C_4/C_3-1)}$$

where

$$C_1 = \frac{-H*a}{D_n\ (a^2 - (L_n)^{-2})}$$

$$C_2 = \{D_n *(-a) + S_n\} \exp(-aB)$$

$$C_3 = \{D_n *(1/L_n) + S_n\} \exp(B/L_n)$$

$$C_4 = \{D_n *(-1/L_n) + S_n\} \exp(-B/L_n)$$

---

*(cont.) The distribution of the minority carrier density is complex due to the range of wavelengths in AM0 light, as it is discussed elsewhere. If we make the simplifying assumption that the distribution goes linearly from its maximum value at the center of a wall to zero at the junction, about 5 microns away, we find that n = .15 x $10^{13}/cm^2$ The doping level for 1 ohm-cm p-type silicon is about 2 x 10^{16} acceptors/cm^3 -- three orders of magnitude greater.

The short circuit current per wavelength, λ, is

$$\frac{dI}{d\lambda} = -qL^2 D_n \left.\frac{dn}{dx}\right|_{x=0,\ \text{junction}}$$

where L^2 = surface area of the plane

q = charge per carrier ($1.6 * 10^{-19}$ coulombs).

Using

$$n = C_1 \{\exp(-ax) + \left(\frac{C_4 - C_2}{C_3 - C_4}\right) * \exp(x/L_n) + \left(\frac{C_3 - C_2}{C_4 - C_3}\right) * \exp(-x/L_n)\}$$

we have

$$\frac{dI}{d\lambda} = \frac{qI^2 Ha}{\{a^2 - (L_n)^{-2}\}} * \{-a + \frac{(C_4 - C_2) + (C_3 - C_2)}{L_n (C_3 - C_4)}\}$$

A program was written to compute the expression $\frac{dI}{d\lambda}$ for a range of diffusion lengths and for various back surface recombination velocities.

The input consisted of a list of how many photons are in each wavelength range, hence, in each range of absorption depth. The number of photons in each wavelength range was calculated from the Solar Spectral Irradiance - Standard Curve by Thekaekara (Ref. 10) using

Energy per photon = hc/wavelength

A smooth curve fit to the data of Dash and Newman (Ref. 11) and Phillip and Ehrenreich (Ref. 12) (see Appendix A) provided an absorption coefficient for each .01 micron wavelength band.

The input data of the absorption coefficients and the number of photons in each wavelength band is tabulated in Appendix A. Also in Appendix A are the results of a program that calculated the distribution of generated carriers. The distribution can be used to find the amount of light absorbed in a plane of a certain thickness even though it is not explicitly needed to calculate $\frac{dI}{d\lambda}$.

A selected portion of the output for the computation of $\frac{dI}{d\lambda}$ is listed in Table 1.

TABLE 1

FLAT CELL SHORT CIRCUIT CURRENT FOR VARIOUS DIFFUSION LENGTHS OVER EIGHT WAVELENGTH BANDS

AMO illumination, no reflection
2 x 2 cm area, 250 microns thick

	L_n (cm)				
wavelength	.04	.0126	.004	.00126	.0004
1.-1.09	.0103	.0075	.0035	.0012	.0004
.9-.99	.0225	.0188	.0112	.0058	.0022
.8-.89	.0262	.0244	.0198	.0125	.0058
.7-.79	.0294	.0285	.0257	.0198	.0115
.6-.69	.0308	.0307	.0296	.0256	.0182
.5-.59	.0311	.0310	.0302	.0282	.0234
.4-.49	.0266	.0265	.0264	.0257	.0240
.3-.39	.0110	.0110	.0110	.0110	.0110
Total (ma)	.1879	.1784	.1574	.1298	.0965

This is for a planar cell 250 microns thick with a back surface recombination velocity of 10^3 cm/sec.

The total current versus diffusion length for a planar cell is compared to a vertical junction cell in Figures 10 and 11.

For light hitting perpendicular to a double planar junction, shown below, the current can be found by changing the boundary conditions on the planar cell equation. Instead of a back surface recombination velocity, one uses zero carrier density at the back surface for a junction short circuited.

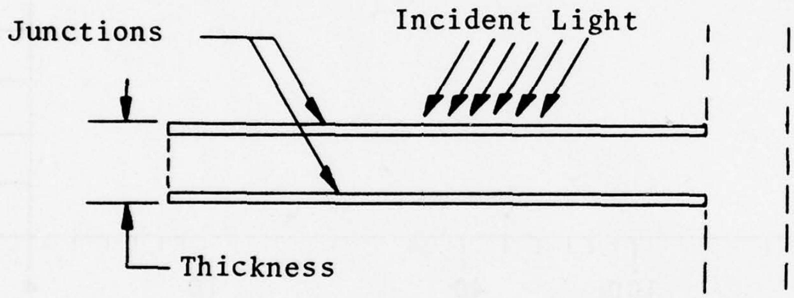

The current at the front surface was found to be proportional to

$$A\{-a + K(\exp(-B/L_n) - \exp(-ab)) + K[\exp(B/L)*n - \exp(-ab)]\}$$

where

$$K = 1/L_n \{\exp(B/L_n) - \exp(-B/L_n)\};\ A = \frac{a}{\{a^2 - (L_n)^{-2}\}}$$

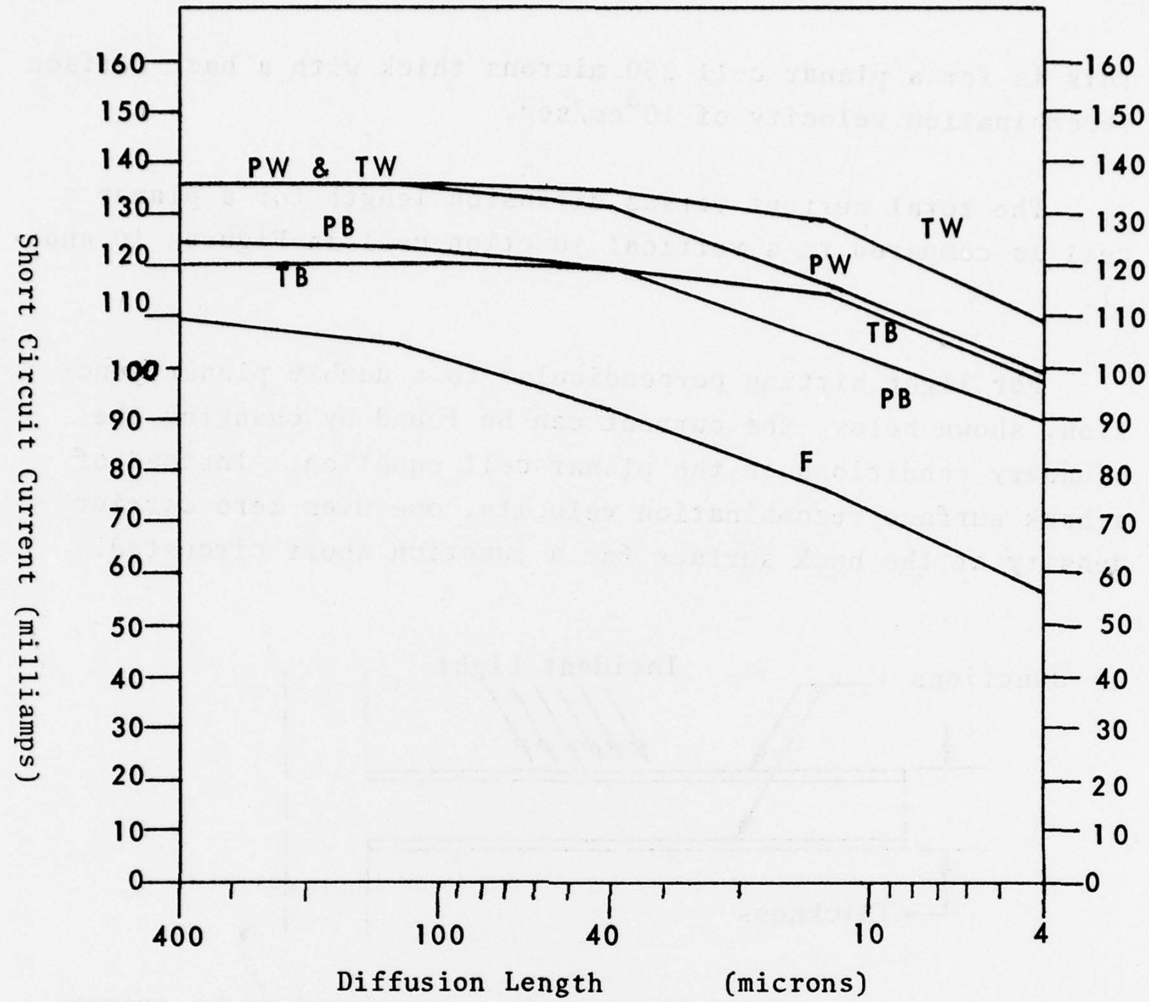

Figure 10: Short Circuit Current Versus Diffusion Length. Comparison of Planar Cell and Vertical Junction Cell Without AR-coating.

Key: F - Flat cell.

P - Much light hits bottom of groove, perpendicular illumination.

T - Most light does not reach bottom of groove, e.g. tilted cell.

B - Much scattered light lost to bulk.

W - Most scattered light absorbed by wall.

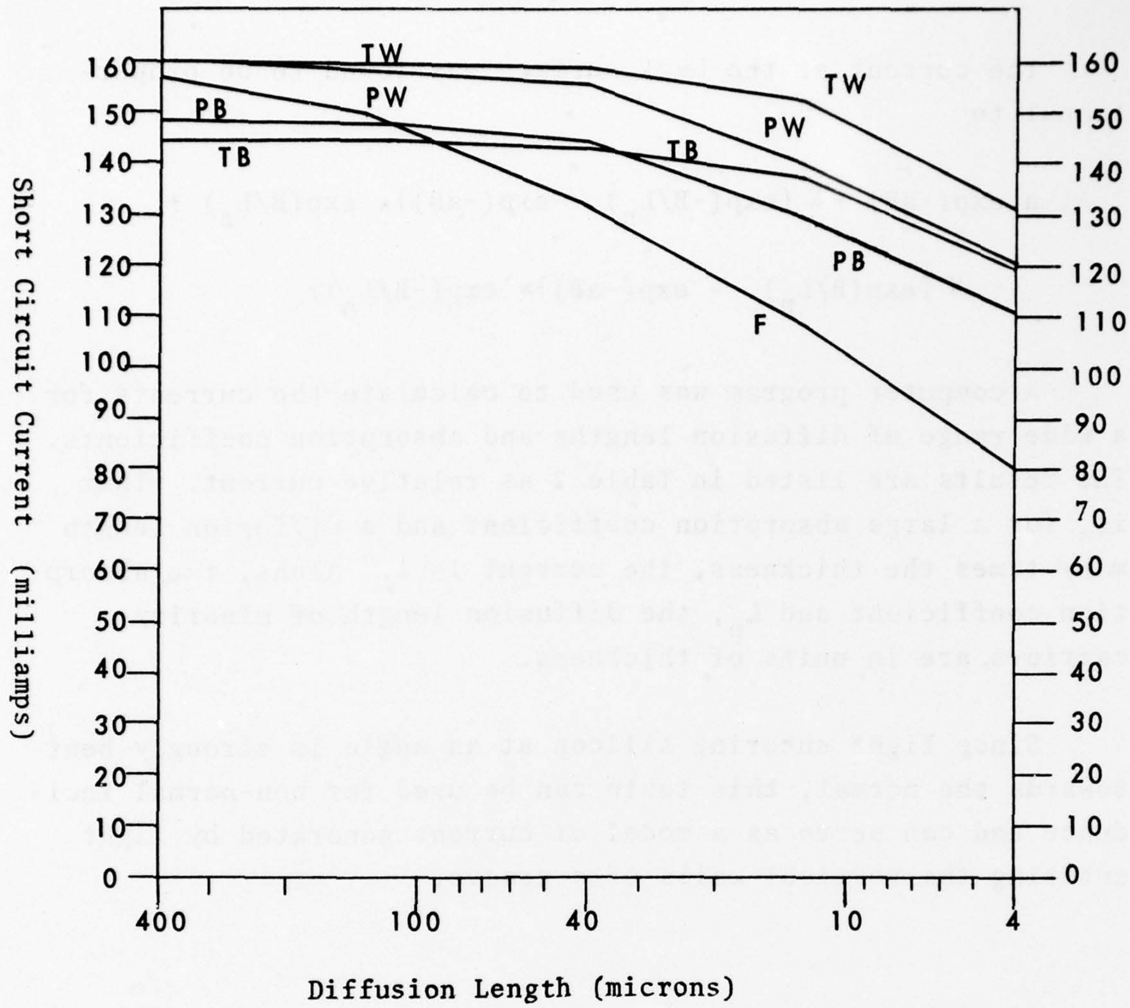

Figure 11: Short Circuit Current Versus Diffusion Length Comparison of Planar Cell and Vertical Junction Cell with AR-Coating.

Key:
F - Flat cell.
P - Much light hits bottom of groove, perpendicular illumination.
T - Most light does not reach bottom of groove, e.g., tilted cell.
B - Much scattered light lost to bulk.
W - Most scattered light absorbed by wall.

The current at the back surface was found to be proportional to

$$A\{-a\ \exp(-aB) + K\ \{\exp(-B/L_n) - \exp(-aB)\} * \exp(B/L_n) +$$

$$K\ \{\exp(B/L_n) - \exp(-aB)\} * \exp(-B/L_n)\}$$

A computer program was used to calculate the currents for a wide range of diffusion lengths and absorption coefficients. The results are listed in Table 2 as relative current. That is, for a large absorption coefficient and a diffusion length many times the thickness, the current is 1. Alpha, the absorption coefficient and L_n, the diffusion length of minority carriers, are in units of thickness.

Since light entering silicon at an angle is strongly bent towards the normal, this table can be used for non-normal incidence and can serve as a model of current generated by light entering the vertical walls of a groove.

TABLE 2

RELATIVE CURRENT OF A VERTICAL JUNCTION ILLUMINATION FROM A SIDE, ARRAYED BY DIFFUSION LENGTH AND LIGHT ABSORPTION COEFFICIENT

<u>KEY</u>: L_n = Diffusion length in units of cell thickness

α = Absorption length in units of inverse cell thickness

Front Current
Back Current
Total Current

GEOMETRY:

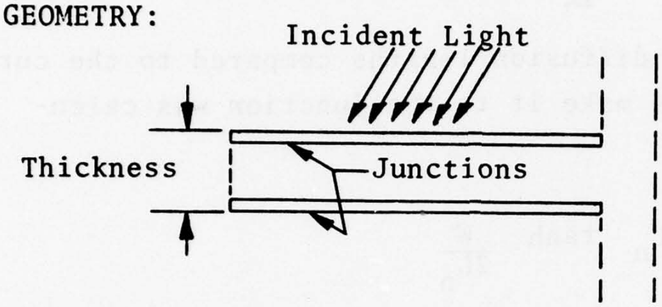

L_n	.05	.1	.2	.5	1.	2.	5.	10.	20.
	.025	.048	.094	.213	.368	.567	.801	.900	.950
20.	.025	.047	.087	.180	.264	.297	.192	.100	.050
	.050	.095	.181	.393	.632	.864	.993	1.00	1.00
	.025	.048	.094	.213	.368	.567	.801	.900	.950
10.	.024	.046	.087	.180	.264	.297	.192	.100	.050
	.049	.094	.181	.393	.632	.864	.993	1.00	1.00
	.0245	.048	.093	.212	.367	.566	.800	.899	.949
5.	.024	.046	.086	.180	.264	.296	.191	.099	.050
	.048	.094	.179	.392	.631	.862	.991	.998	.999
	.024	.047	.092	.208	.361	.559	.793	.894	.946
2.	.024	.046	.086	.176	.258	.289	.185	.096	.048
	.048	.093	.178	.384	.619	.848	.978	.990	.994
	.023	.045	.087	.198	.343	.535	.769	.877	.937
1.	.022	.043	.081	.166	.241	.268	.168	.086	.043
	.045	.088	.168	.364	.584	.803	.937	.963	.980
	.019	.037	.072	.165	.290	.462	.697	.825	.905
.5	.018	.035	.066	.135	.193	.208	.120	.057	.028
	.037	.072	.138	.300	.483	.670	.817	.882	.933
	.0098	.019	.038	.090	.165	.285	.500	.666	.800
.2	.0095	.018	.033	.066	.089	.084	.030	.009	.0036
	.020	.037	.071	.156	.254	.369	.503	.675	.804
	.0050	.0099	.020	.048	.091	.166	.333	.500	.666
.1	.0048	.0091	.017	.032	.041	.034	.007	.0004	.0001
	.010	.019	.037	.080	.132	.200	.340	.500	.666
	.0025	.0050	.0099	.024	.048	.091	.200	.333	.500
.05	.0024	.0045	.0083	.0155	.019	.015	.002	.0001	.0000
	.005	.009	.018	.039	.067	.106	.202	.333	.500

For this kind of structure, with no junction on top,

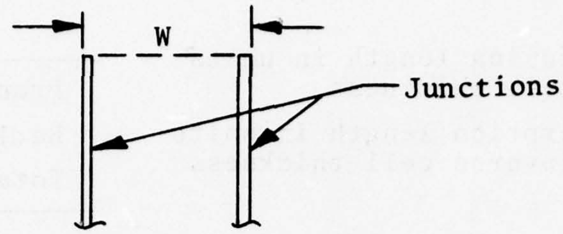

the current for various diffusion lengths compared to the current if all the carriers make it to the junction was calculated to be

$$2L_n \tanh \frac{W}{2L_n}$$

This expression can be derived from the formula for a double planar junction by letting the absorption coefficient go to zero, while the intensity goes to infinity such that their product goes to one. Taking such a limit represents an illumination that is even with respect to distance in the w direction.

The total current into both junctions for L_n in units of w is listed below in Table 3.

TABLE 3

CURRENT FOR PARALLEL JUNCTIONS WITH ILLUMINATION THAT IS UNIFORM WITH RESPECT TO DISTANCE FROM THE JUNCTION

L_n	.1	.2	.5	1.	2.	5.	10.
I_{sc}	.2	.39	.76	.92	.98	1.	1.

2. Theoretical Electrical Performance

The information developed in the previous section can be used to estimate the performance of a vertical junction cell. The procedure can be outlined as follows. The light that isn't reflected from the metal contacts either impinges upon the top edge of a vertical wall or enters a groove. Some of the light that impinges upon a wall edge is reflected and some absorbed. The photons that are absorbed through a wall edge create carriers that can be collected by either the junction on the top edge or the vertical walls. Some of the light that enters a groove is reflected, but most is absorbed by the wall or by the groove bottom. After the light has been partitioned, the carrier collection efficiency for the basic geometries can be used to find currents, which sum to the short circuit current of a vertical junction cell. This procedure will be described in more detail below and then developed mathematically. The open circuit voltage will be discussed, and it is shown that the voltage of a vertical junction cell could be nearly equal to a flat cell of the same resistivity. A specific example will be used in which the mask has five micron windows for etching grooves and ten microns between windows.

A vertical junction cell can be divided into three regions: the flats (including ribs between grooved regions) where silver contacts are deposited; the edges of the vertical walls; and the grooves. The flats within this approximation, comprising about 10% of the area, are mostly shadowed with silver and will be considered inactive. When etching preferentially to a depth of 100 microns, an undercutting of one micron on either side can be expected (Ref. 9).

Windows opened to about seven microns and walls correspondingly reduced suggest that for this example the 90% of the light hitting the grooved region can be divided evenly into light entering the top edge of the walls and light entering the grooves.

The light that enters the top edge of a wall is totally internally reflected by the vertical silicon-vacuum or silicon-silicone rubber interface and, hence, remains in the wall. For light entering the top plateau of a wall, the generated carriers are either collected by the top junction, or those not collected there are collected by the side walls. For an angle of incident illumination nearly normal to the surface, the percentage of carriers collected by the top plateau is the ratio of current from a flat cell, Table 1, to the theoretical maximum of 206 ma/4 sq cm (206 ma = total number of photons x charge). The carriers not collected by the top of the wall are collected by the side junctions with an efficiency of $2\ L_n \tanh w/2L_n$. Carriers from infrared light are an exception in that many are generated beneath the wall. By the time light has penetrated the wall height, 100 microns, the photons remaining are mostly infrared and will go deep into the bulk. These photons penetrating beneath the walls will be given up for lost. They are about 9% of the total. Table A, in Appendix A, lists the cumulative number of carriers generated within a slice of silicon for a range of thicknesses. This can be converted to a table showing the percent of photons not absorbed for various wall heights (see Table 4).

TABLE 4

PERCENT OF PHOTONS NOT ABSORBED FOR VARIOUS WALL HEIGHTS

Height of wall (μm)	Percent of photons not absorbed in wall
5	45%
10	31%
20	22%
50	14%
100	9%
200	5%

The total energy entering the wall tops is lessened by reflection: from 35% from bare silicon to 7% from a single layer anti-reflection (AR) coated surface. The AR-coating is frequency dependent with a bandwidth of about one octave which is a little narrower than the range of frequencies for which the cell is sensitive. One could choose to absorb the blue at the expense of reflecting the infrared that penetrates below the walls. The best AR-coating can be determined experimentally. This study will simply describe the light entering the wall tops as reduced in intensity over all wavelengths by either 7% or 35%.

For light that enters a groove, it is difficult to say exactly where it enters the silicon. One might suppose that vertical illumination would allow light to enter the bottom rather than the sides, while for illumination from a slight angle, the light would enter the walls as shown below.

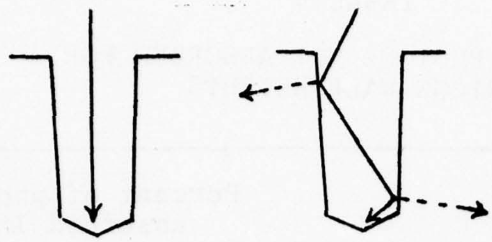

Yet even with vertical illumination, some light would scatter from the bottom and enter the sides (as much as 35% on a non-AR coated bottom). Furthermore, a 7.5 micron groove presents an aperture about 10 wavelengths wide, so that the 100 microns to the bottom of a groove allows dispersion due to the wave nature of the light. Hence, for the case of perpendicular illumination, less light reaches the bottom than simple ray tracing would indicate.

The exact distribution of generated carriers is impossible to determine without a detailed analysis of the manner of reflection off the wall and bottom and an analysis of interference effects. The quantity of light absorbed in the walls versus the bulk below the grooves will be left as an uncertainty in the range of say, 5% to 30% reaching the groove bottom, depending in practice on whether the bottom or side walls are AR-coated, the tilt angle of the cell, and the actual slope of the walls.

A cell tilted slightly, 10%, has the light making several reflections from the side-wall, allowing several opportunities for absorption. Note that the area as seen by the sun for a cell tilted 10° is cosine 10° = .985, i.e., only 1.5% less than a cell directly facing the sun.

In practice, the grooves appear black so it will be assumed that 95% of the light entering a vertical groove is absorbed and 5% is reflected back into space.

It will be assumed that the light that enters the bottom of the groove supplies current with the same functional dependence on diffusion length as a flat cell. This approximation is valid until the diffusion length is reduced to the same order of magnitude as the wall width. To remove such over-optimism, the collection efficiency for light entering the bottom of a groove will be taken as half that of a flat cell when the diffusion length becomes less than twice the groove width.

The light entering a smooth side-wall is strongly bent towards the normal. Silicon's index of refraction is about four, which implies that the angle is always less than 14° = (arcsin 1/4) from the normal. So Table 2 can be used to calculate the current by dividing AMO light into bands of various absorption depths as in Table 5. The case of a textured wall, whereby the light might be scattered as it enters, is not considered because of the extreme difficulty in handling such a case.

TABLE 5

RELATIVE DISTRIBUTION OF PHOTONS FOR EIGHT WAVELENGTH BANDS AND AN ABSORPTION COEFFICIENT FOR EACH BAND

Wavelength band	% of total number of photons in .3-1.1 μm band	Absorption coefficient α (cm^{-1})
.3-.39	5.3	10^7
.4-	12.8	$2x10^4$
.5-	15.0	$7x10^3$
.6-	15.8	$3x10^3$
.7-	14.7	$1.5x10^3$
.8-	13.4	600.
.9-	12.2	200.
1.-1.09	10.8	30.

Some light exits the wall after passing through it. Where it goes from there is difficult to predict as it greatly depends on the texture and slope of the wall surfaces it has passed through. This light is predominantly of wavelengths which have an absorption depth longer than one wall thickness, so it can be described as giving an infrared background evenly spread throughout the silicon. Hence, it will be assumed that the efficiency of collection for light that has passed through a wall goes as $2L_n \tanh (w/2L_n)$ while either 25% or 75% (a wide range, admittedly) of this is lost by entering the bulk below the grooves. The amount penetrating further than one wall thickness can be found from Table 9 as being between 31% and 45% of the total striking the walls. Including the light internally reflected in the wall, the light not absorbed will be taken as 37%.

Using Table 2 to calculate the current due to light absorbed by a wall, one must first express the absorption coefficents of Table 5 in units of wall width. For 7.5 μm walls, these are:

wavelength band	.3-.39	.4-	.5-	.6-	.7-	.8-	.9-	.1-1.09
absorption coefficient	7500	15	5.25	2.25	1.125	.45	.15	.0225

As an example, for a diffusion length long compared to wall width, one can use the row $L_n = 20$ of Table 2 and calculate the percent of photons converted to current as shown in Table 6.

TABLE 6

SAMPLE CALCULATION OF CARRIER COLLECTION EFFICIENCY FOR VERTICAL WALL ILLUMINATED ON ONE SIDE

Wavelength Band	Collection Efficiency	% of photons in band	% of carriers collected
.3-.39	1.	5.3	5.3
.4-.49	1.	12.8	12.8
.5-.59	1.	15.	15.0
.6-.69	.86	15.8	13.6
.7-.79	.63	14.7	9.2
.8-.89	.39	13.4	5.2
.9-.99	.15	12.2	1.8
1.-1.09	.02	10.8	.2
		Total	63.1%

Long diffusion length means good carrier collection efficiency so that most of the current not collected, 36.9%, was never absorbed in the walls, in agreement with the 37% chosen from Table 4.

Five sample values will be used for diffusion lengths:

400, 125, 40, 12.5, and 4 microns

Expressed in units of wall width these are (in the same order):

53.5, 16.6, 5.3, 1.6, and .53.

The results of using Table 2 to calculate relative current for these diffusion lengths are:

63%, 63%, 62%, 60%, and 51% carrier collector efficiency.

At first glance, one might wonder why the reduction of current as diffusion length decreases to less than the wall width is only from 64% to 51%. The explanation is that much of the AMO light has an absorption depth shorter than even the 4 micron diffusion length, hence, AMO light generates carriers very near the junction which are always collected. Also, much of the light that reaches the center of the wall has an absorption depth longer than a wall width which sets 63% as the upper limit.

This discussion can be put into the following mathematical formula:

Current = (Max.) (.9) (.5Q + .5T)

Max. = 100% quantum efficiency current

.9 = metallic shadow

.5 = 50/50 groove/wall

Q = Quantum efficiency of groove

T = Quantum efficiency of light entering top edge of wall

$T = AR\ (F + (1\text{-}F)\ (tanh))(.91)$

AR = .93 or .65, anti-reflection coating

F = Quantum efficiency of flat cell

$tanh = 2L_n\ \tanh\ (w/2L_n)$ wall with illumination uniform with respect to side junctions

.91 = finite wall height

$Q = .95\ (PT(F/I) + (1\text{-}PT)\ \{S + .37\ (tanh)\ BW\})$

.95 = 5% reflected from groove

PT = .05 or .3, light entering bottom of groove

F = Quantum efficiency of flat cell

I = 1, unless diffusion length < wall width in which case I = 2

S = Quantum efficiency of light entering sidewalls, .63-.51 depending on diffusion length

.37 = Light exiting sidewalls

BW = .25 or .75, scattered light lost to bulk below grooves

The results for the various conditions are plotted in the graph of Figures 10 and 11. Also plotted is the current of a flat cell with the same quantity of metallization shadowing, 10%, as is assumed for the vertical junction cell. Figure 10 is for AR-coated cells and Figure 11 is for non-AR versions of the same cells.

For a flat cell, the open circuit voltage can be calculated from

$$V_{oc} = (kT/q)\ \ln\ (I_{sc}/I_o)$$

where

$$I_o = \frac{Aq\ n_i^2 D_n}{N_A L_n}$$

Using

$$I_{sc} = 160 \text{ ma}$$

$$D_n = 34 \text{ cm}^2/\text{sec}$$

$$L_n = 250 \text{ microns}$$

$$N_A = 6 \times 10^{15}/\text{cm}^3$$

for 2 ohm-cm material. We have:

$$I_o = 2.176 \times 10^{-11} \text{ and } V_{oc} = 591 \text{ mV}$$

Towards the end of life, L_n goes down by a factor of 50 to 5 microns, and the current goes down by a factor of two. The result is an open circuit voltage of 471 mV for a flat cell.

Even though the area of a vertical junction cell is at least ten times greater than a flat cell, the reverse current does not increase appreciably, since the vertical walls are "flooded" with injected minority carriers. The concept of flooding is discussed in a paper by J. Lindmayer (Ref. 13). What happens in a vertical junction cell with a wall width less than the diffusion length is that an injected carrier will diffuse back to the junction as if it was photo-generated so that the only sink is the bottom of the grooves, the same area as a flat cell.

3. Diffusion Length after Damaging Radiation

The diffusion length of minority carriers after a given dose of radiation is a function of several variables such as initial diffusion length, resistivity, and crystal impurities, e.g., quantity of oxygen. Table 7 summarizes several studies of the minority carrier diffusion length damage constant, K_L, at the energies specified in the contract for a p-type bulk.

K_L is defined as:

$$(1/L_n)^2 - (1/L_o)^2 = \Phi K_L$$

where

Φ = accumulated radiation dose

L_o = initial minority carrier diffusion length

L_n = final minority carrier diffusion length

The worst case diffusion lengths at the highest requested fluence levels (assuming $1/L_o$ is negligible) are (from Table 7):

For 5×10^{15} 1MeV electrons/cm^2 with $K_L = 8 \times 10^{-10}$, L=5 microns;

For 10^{12} 10 MeV protons/cm^2 with $K_L = 1.3 \times 10^{-6}$, L=8.2 microns;

For 3×10^{12} 1 MeV neutrons/cm^2 with $K_L = 5 \times 10^{-7}$, L=8.2 microns.

Values of L_n are within the range of the performance graphs, Figures 10, 11, and 12.

TABLE 7

DIFFUSION LENGTH DAMAGE CONSTANT K_L FOR 1 MeV ELECTRONS 10 MeV PROTONS, AND 1 MeV EQUIVALENT NEUTRONS

K_L	Remarks	Reference
1 MeV Electrons		
1.5×10^{-10}	1 ohm-cm	14
2×10^{-11}	10 ohm-cm float zone	16
10^{-10}	1 ohm-cm FZ	16
4×10^{-10}	.1 ohm-cm FZ	16
4×10^{-11}	10 Ohm-cm Czochralski	16
2×10^{-10}	1. ohm-cm CZ	16
8×10^{-10}	.1 ohm-cm CZ	16
10 MeV Protons		
2×10^{-7}	10 ohm-cm	16
5×10^{-7}	1 ohm-cm	16
1.3×10^{-6}	.1 ohm-cm	16
1 MeV Equivalent Neutrons		
5×10^{-7}	1 MeV neutrons	15
1.7×10^{-7}	Fission spectrum 5-10 ohm-cm	17
3.2×10^{-7}	Fission spectrum 2.5 ohm-cm	18

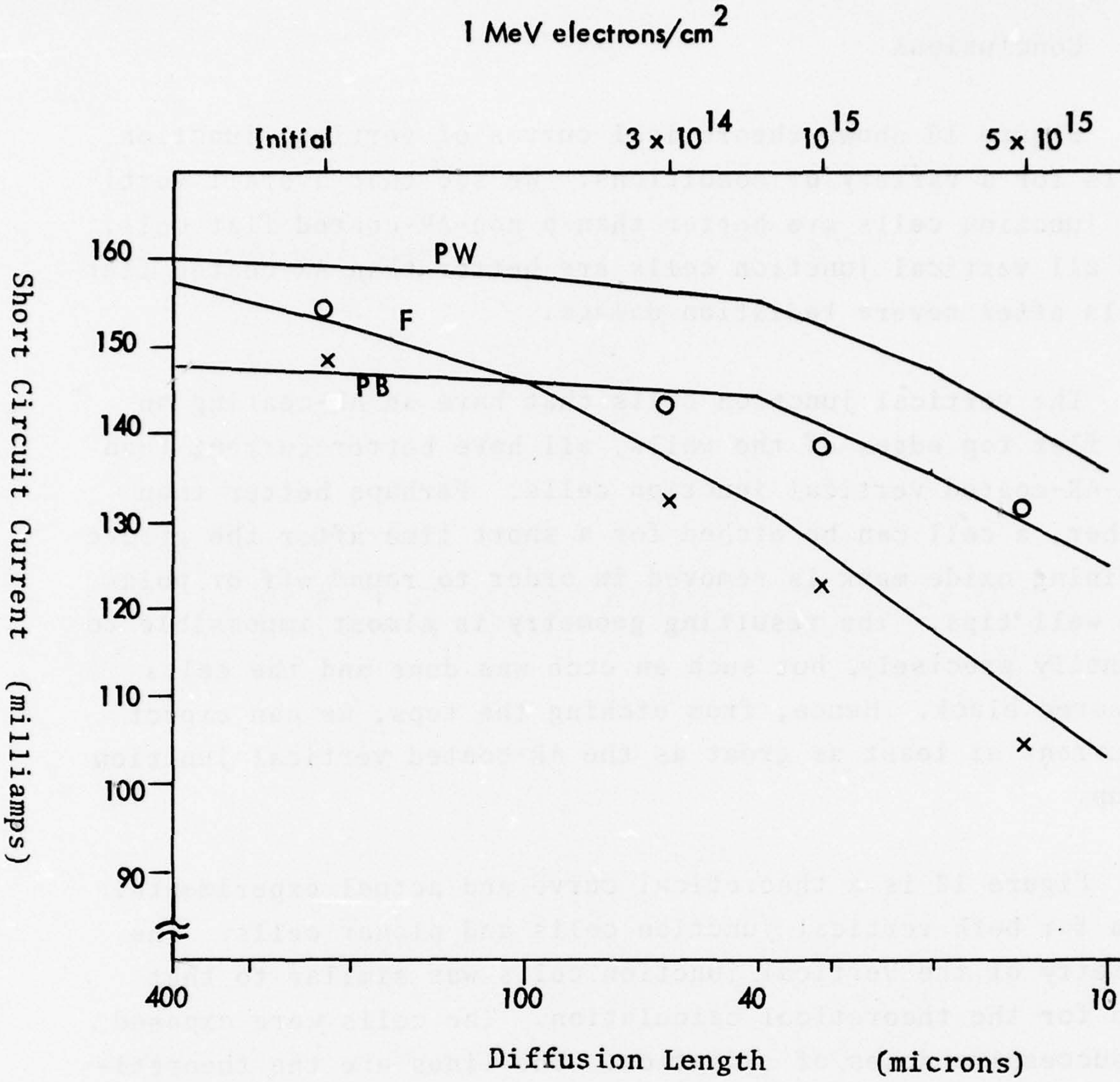

Figure 12: Short Circuit Current Versus Damaging Radiation-Experiment and Theory.

4. Conclusions

Figure 10 shows theoretical curves of vertical junction cells for a variety of conditions. We see that overall vertical junction cells are better than a non-AR-coated flat cell, and all vertical junction cells are better than AR-coated flat cells after severe radiation damage.

The vertical junction cells that have an AR-coating on the flat top edges of the walls, all have better current than non-AR-coated vertical junction cells. Perhaps better than either, a cell can be etched for a short time after the groove-defining oxide mask is removed in order to round off or point the wall tips. The resulting geometry is almost impossible to quantify precisely, but such an etch was done and the cells appeared black. Hence, from etching the tops, we can expect a current at least as great as the AR-coated vertical junction group.

Figure 12 is a theoretical curve and actual experimental data for both vertical junction cells and planar cells. The geometry of the vertical junction cells was similar to that used for the theoretical calculation. The cells were exposed to successive doses of radiation. The lines are the theoretical values, while the circles are the experimental data. The radiation dose has been related to the corresponding diffusion length using the assumption that the L_o term is negligible and using the value of $K_L = 10^{-10}$ which is appropriate for the 2 ohm-cm silicon used. The accuracy of these assumptions is indicated by the close fit between the theoretical curves and the actual experimental points for the planar cell. There is not enough experimental data available yet to make a precise comparison with the theory, but the initial values show good agreement.

The theoretical analysis shows that, indeed, the vertical junction cell shows a vastly improved radiation resistance. We can now use the theoretical calculations to determine how to improve the radiation resistance of the vertical junction cells. Since light that enters the bulk below the grooves behaves exactly like a planar cell, the most radiation resistant cell will have narrower groove bottoms so that more light can enter the walls. Because the percent reflected from the silicon surface is so important for the amount absorbed in the walls, the walls should be tapered to improve the absorption.

Another area of interest is non-normal incident. A slight tilt of, say, 10° from the sun would reduce the incident solar energy by only 1.5%, yet would allow considerably more light to be absorbed in the walls rather than reaching the bottom of the grooves. Therefore, for maximum efficiency as the total dose of radiation increases, the cell should be tilted so that a larger portion of the carriers are generated in the walls.

IV. EXPERIMENTAL RESULTS

1. I-V Characteristics

Vertical junction cells with the 7 buss bar geometry have been fabricated with AMO efficiencies of greater than 13%. Figure 13 shows the I-V characteristics indicative of the best cells produced to date. Short circuit currents of 160 milliamperes have been obtained consistently. The open circuit voltage for these cells was 570 millivolts with a fill factor of .79. These cells have been produced on silicon with resistivities between 1.5 and 2.5 ohm-cm, so the voltage is not appreciably lower than for similar resistivity planar cells.

One major misconception about vertical junction cells has been erased by the development of these cells. It was initially believed that the vertical junction solar cells would exhibit low photovoltages due to the large reverse saturation current, which should be proportional to junction area. This area effect should be drastic for the vertical junction cell because the area is 10 to 20 times that of a planar cell. However, our data show that photovoltage is not appreciably reduced from the planar values. Direct measurements in the dark show that the reverse saturation current is not significantly higher for the vertical junction cells. The explanation for the lower reverse saturation current is flooding of the thin walls by the minority carriers from the N^+ diffused regions. Therefore the recombination of these minority carriers will be less than if there was an infinite bulk behind the junction. With this reduction in reverse saturation current in the walls, the photovoltage will be higher than that expected from simple area scaling.

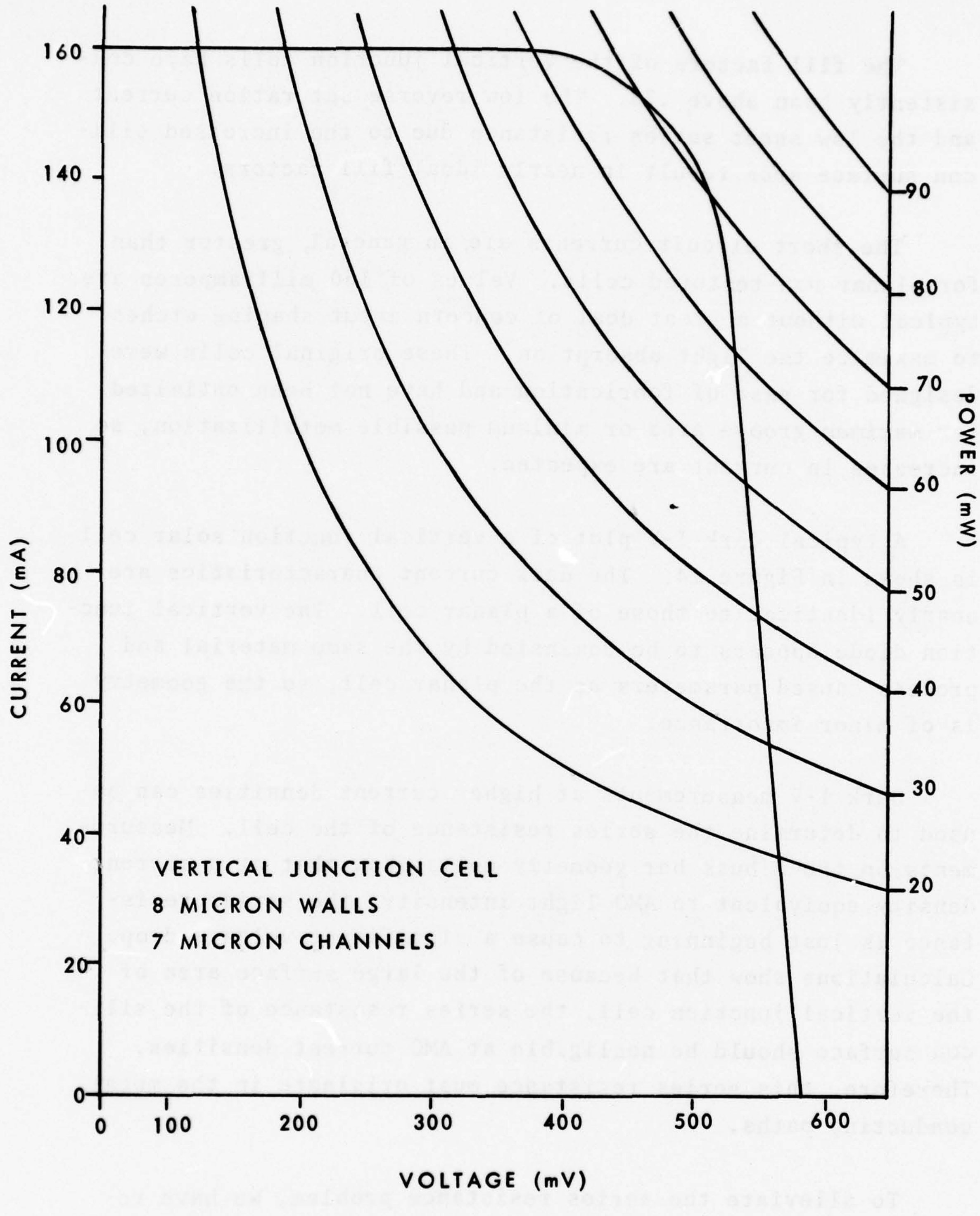

Figure 13: I-V Characteristics at AM0 for a Vertical Junction 2cm x 2cm Solar Cell.

The fill factors of the vertical junction cells have consistently been above .78. The low reverse saturation current and the low sheet series resistance due to the increased silicon surface area result in nearly ideal fill factors.

The short circuit currents are, in general, greater than for planar non-textured cells. Values of 160 milliamperes are typical without a great deal of concern about shaping etches to maximize the light absorption. These original cells were designed for ease of fabrication and have not been optimized for maximum groove area or minimum possible metallization, so increases in current are expected.

A typical dark I-V plot of a vertical junction solar cell is shown in Figure 14. The dark current characteristics are nearly identical to those of a planar cell. The vertical junction diode appears to be dominated by the same material and process caused parameters as the planar cell, so the geometry is of minor importance.

Dark I-V measurements at higher current densities can be used to determine the series resistance of the cell. Measurements on the 7 buss bar geometry cells show that at a current density equivalent to AMO light intensity, the series resistance is just beginning to cause a significant voltage drop. Calculations show that because of the large surface area of the vertical junction cell, the series resistance of the silicon surface should be negligible at AMO current densities. Therefore, this series resistance must originate in the metal conducting paths.

To alleviate the series resistance problem, we have redesigned the cell geometry. The first change was to the 13 buss bar geometry which did alleviate the series resistance

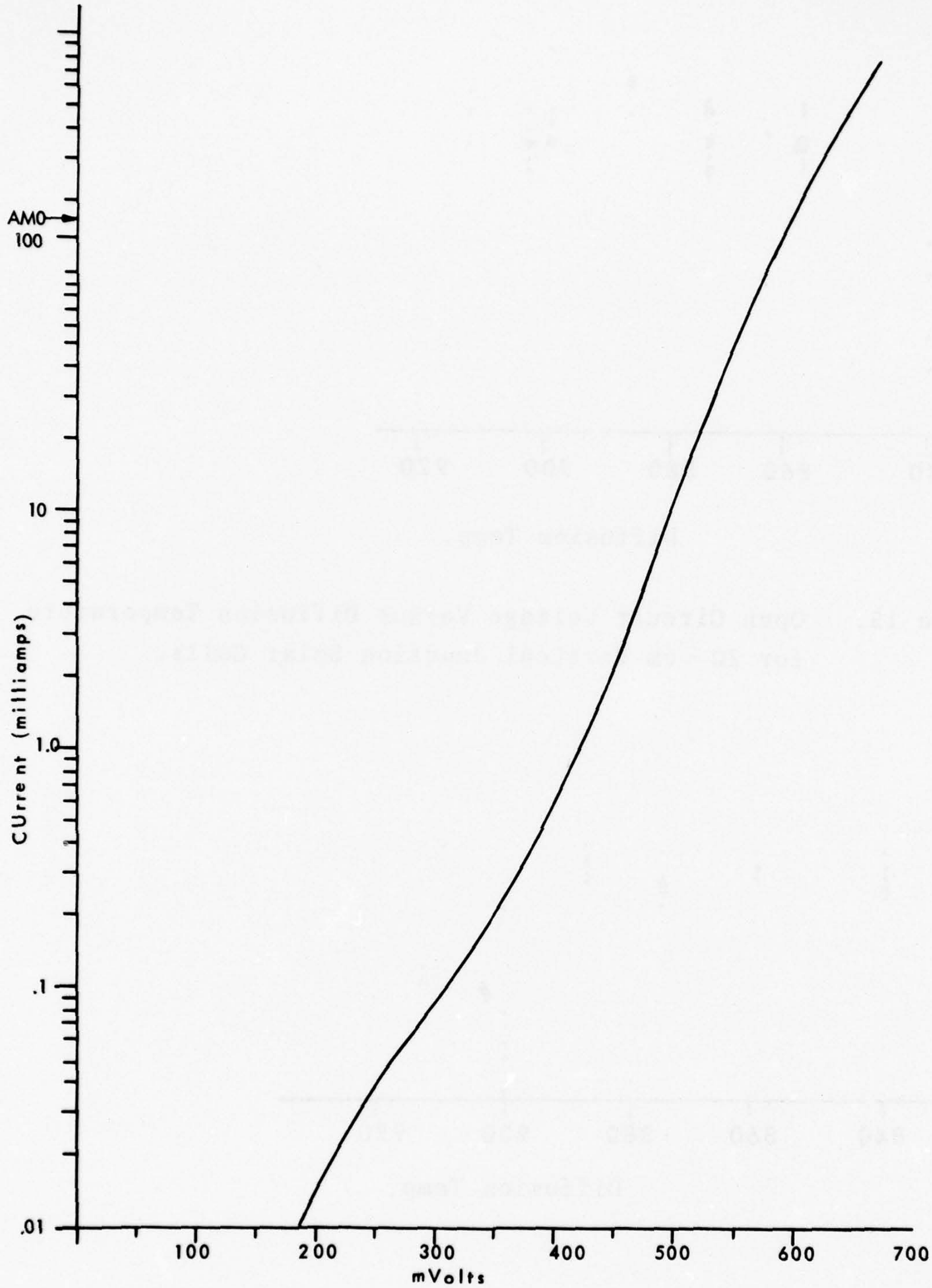

Figure 14: Dark I-V Characteristics for a Vertical Junction 2cm x 2cm Solar Cell

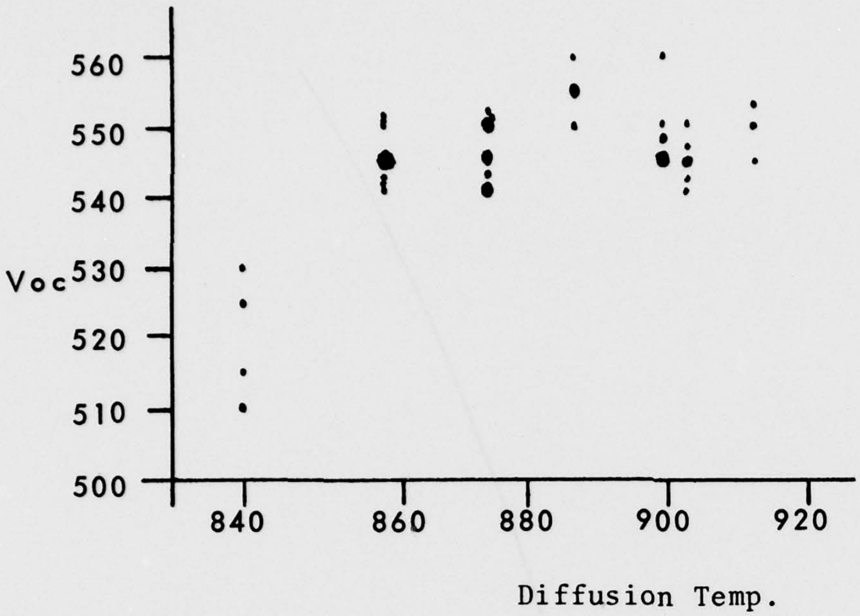

Figure 15: Open Circuit Voltage Versus Diffusion Temperature for 2Ω - cm Vertical Junction Solar Cells.

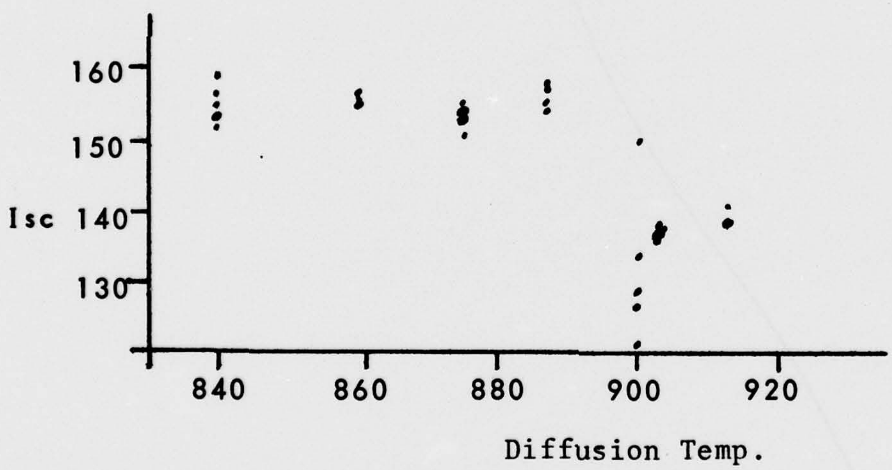

Figure 16: Short Circuit Current Versus Diffusion Temperature for 2Ω - cm Vertical Junction Solar Cells.

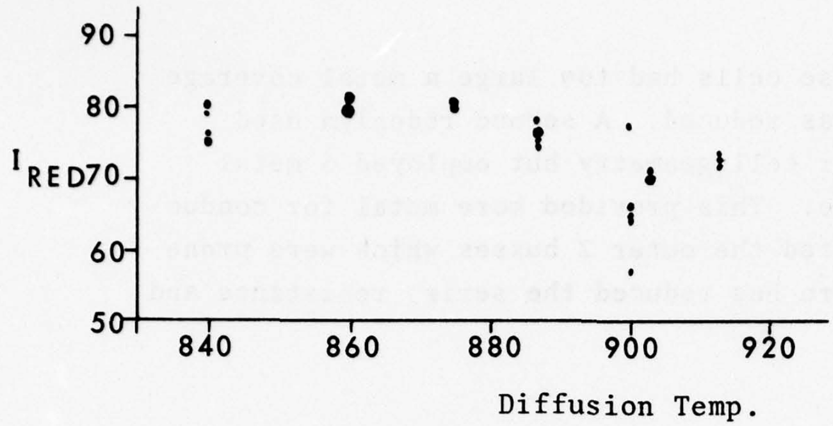

Figure 17: Current with Red Filter Versus Diffusion Temperatures for 2 Ω- cm Vertical Junction Solar Cells.

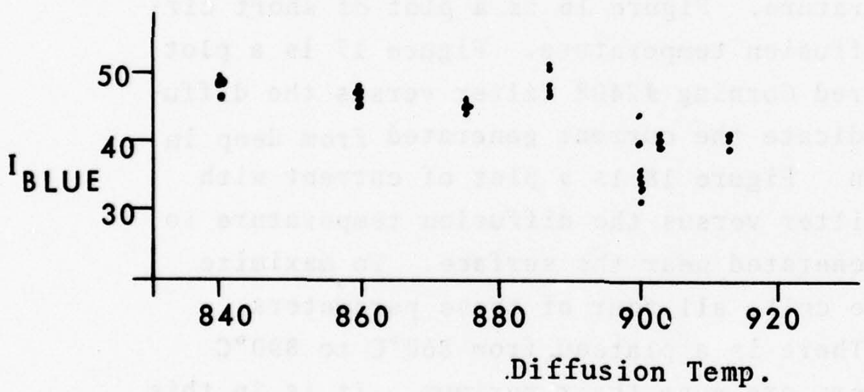

Figure 18: Current with Blue Filter Versus Diffusion Temperature for 2 Ω-cm Vertical Junction Solar Cell.

problem. However, these cells had too large a metal coverage area, so the current was reduced. A second redesign used the original 7 buss bar cell geometry but employed 5 metal grids, each 6 mils wide. This provided more metal for conduction paths and eliminated the outer 2 busses which were prone to damage. This pattern has reduced the series resistance and is now in use.

2. Diffusion Profile

A set of experiments have been performed with the resisttivity of the silicon, and all of the process parameters except diffusion temperature held constant. The cells were co-processed up until the diffusion steps in an attempt to eliminate all variables except for the diffusion temperature. The diffusion termperature was varied from 840°C to 913°C.

The results of these experiments are summarized in Figures 15, 16, 17, and 18. Figure 15 is a plot of open circuit voltage versus diffusion temperature. Figure 16 is a plot of short circuit current versus diffusion temperature. Figure 17 is a plot of the current with a red Corning #2408 filter versus the diffusion temperature to indicate the current generated from deep in the bulk of the silicon. Figure 18 is a plot of current with a blue Corning #9788 filter versus the diffusion temperature to indicate the current generated near the surface. To maximize the power output of the cell, all four of these parameters should be maximized. There is a plateau from 860°C to 890°C where the four parameters are near their maximum. It is in this temperature region that all subsequent diffusions should be performed.

3. Capacitance Measurements

The capacitance of a P-N junction is proportional to the junction area. Therefore, a comparison between the capacitance of a vertical junction and the capacitance of a planar cell will indicate the ratio of the areas of the two cells. The average capacitance of 2 cm x 2 cm planar 1.5 ohm-cm solar cells is about .1 microfarad, while the measured capacitance for a 2 cm x 2 cm vertical junction 1.5 ohm-cm solar cell is 1.0 microfarad. Therefore, the junction area of the vertical junction cells is 10 times greater than the junction area of the planar cell. This is the same ratio as the ratio of the areas of the two cells. This means that all of the surface area of the vertical junction cells has been adequately diffused, so that the junction does indeed follow the walls up and down the narrow grooves. This erases a second major misconception that has been held concerning vertical junction solar cells. The belief was that you could not diffuse uniformly into the narrow grooves. Since our measurements show that the junction has an area equal to the surface area, there is no problem in diffusing into the grooves.

4. Temperature Coefficients

The temperature coefficient of the open circuit voltage and the maximum power have been measured from 20°C to 90°C. The data for open circuit voltage versus cell temperature is plotted in Figure 19. The data for maximum power versus temperature is plotted in Figure 20. The temperature coefficients are:

$$V_{oc} = 2.05 \text{ millivolts/°C}$$

$$P_{sc_{max}} = .275 \text{ milliwatts/°C}$$

These values are not significantly different from those measured for planar cells.

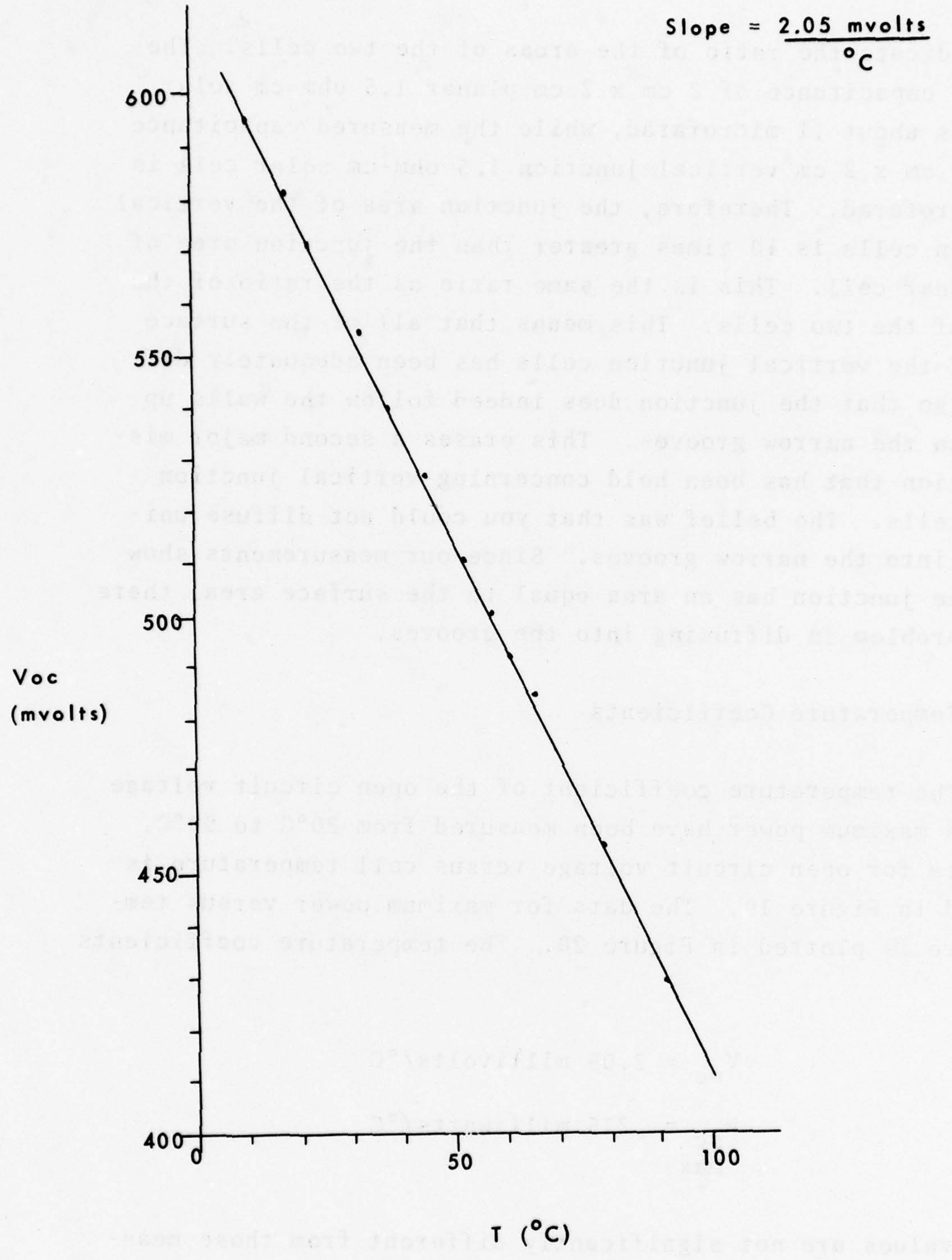

Figure 19: Temperature Variation of the Open Circuit Voltage for a Vertical Junction Solar Cell

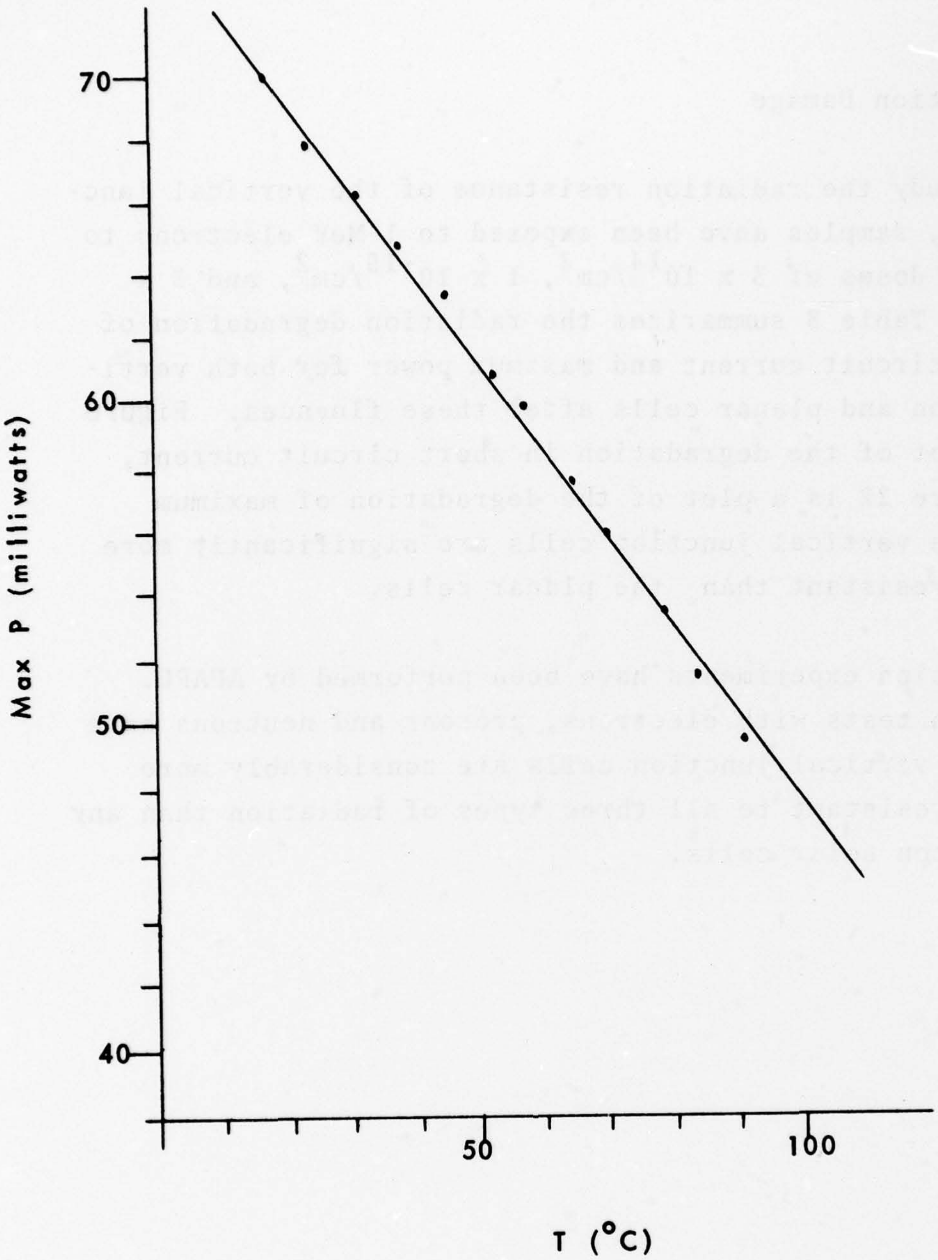

Figure 20: Temperature Variation of the Maximum Power for a Vertical Junction Solar Cell.

5. Radiation Damage

To study the radiation resistance of the vertical junction cells, samples ahve been exposed to 1 MeV electrons to integrated doses of $3 \times 10^{14}/cm^2$, $1 \times 10^{-15}/cm^2$, and $5 \times 10^{15}/cm^2$. Table 8 summarizes the radiation degradation of the short circuit current and maximum power for both vertical junction and planar cells after these fluences. Figure 21 is a plot of the degradation in short circuit current, while Figure 22 is a plot of the degradation of maximum power. The vertical junction cells are significantly more radiation resistant than the planar cells.

Radiation experiments have been performed by AFAPL. Irradiation tests with electrons, protons and neutrons have shown that vertical junction cells are considerably more radiation resistant to all three types of radiation than any other silicon solar cells.

TABLE 8

RADIATION DEGRADATION OF SHORT CIRCUIT CURRENT AND MAXIMUM POWER FOR VERTICAL JUNCTION AND PLANAR SOLAR CELLS (1MeV ELECTRONS)

Vertical Junction Cells

Dose	Isc (mamps)	% Loss in Isc	Max P in watts	% Loss in Max P
Before irradiation	154	--	68	--
3×10^{14}	142	7.8	60	11.8
1×10^{15}	140	9.1	56	17.6
5×10^{15}	134	13.2	50	26.5

Planar Cells

Dose	Isc (mamps)	% Loss in Isc	Max P in watts	% Loss in Max P
Before irradiation	151	--	67.5	--
3×10^{14}	134.5	10.7	56.5	16.3
1×10^{15}	124.5	17.4	52	23.5
5×10^{15}	108	28.4	41	38.6

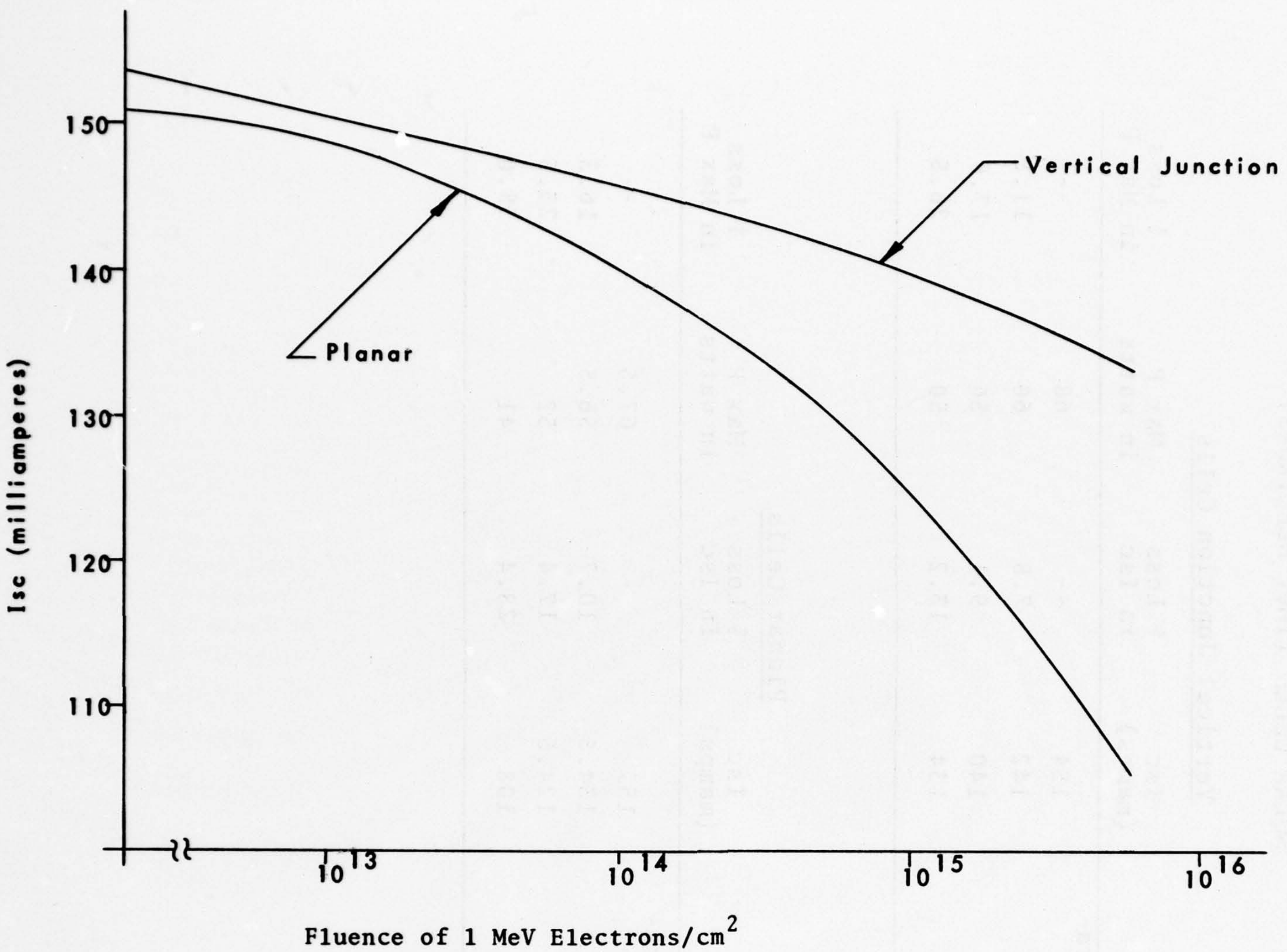

Figure 21: Radiation Degradation of the Short Circuit Current for Vertical Junction and Planar Silicon Solar Cells.

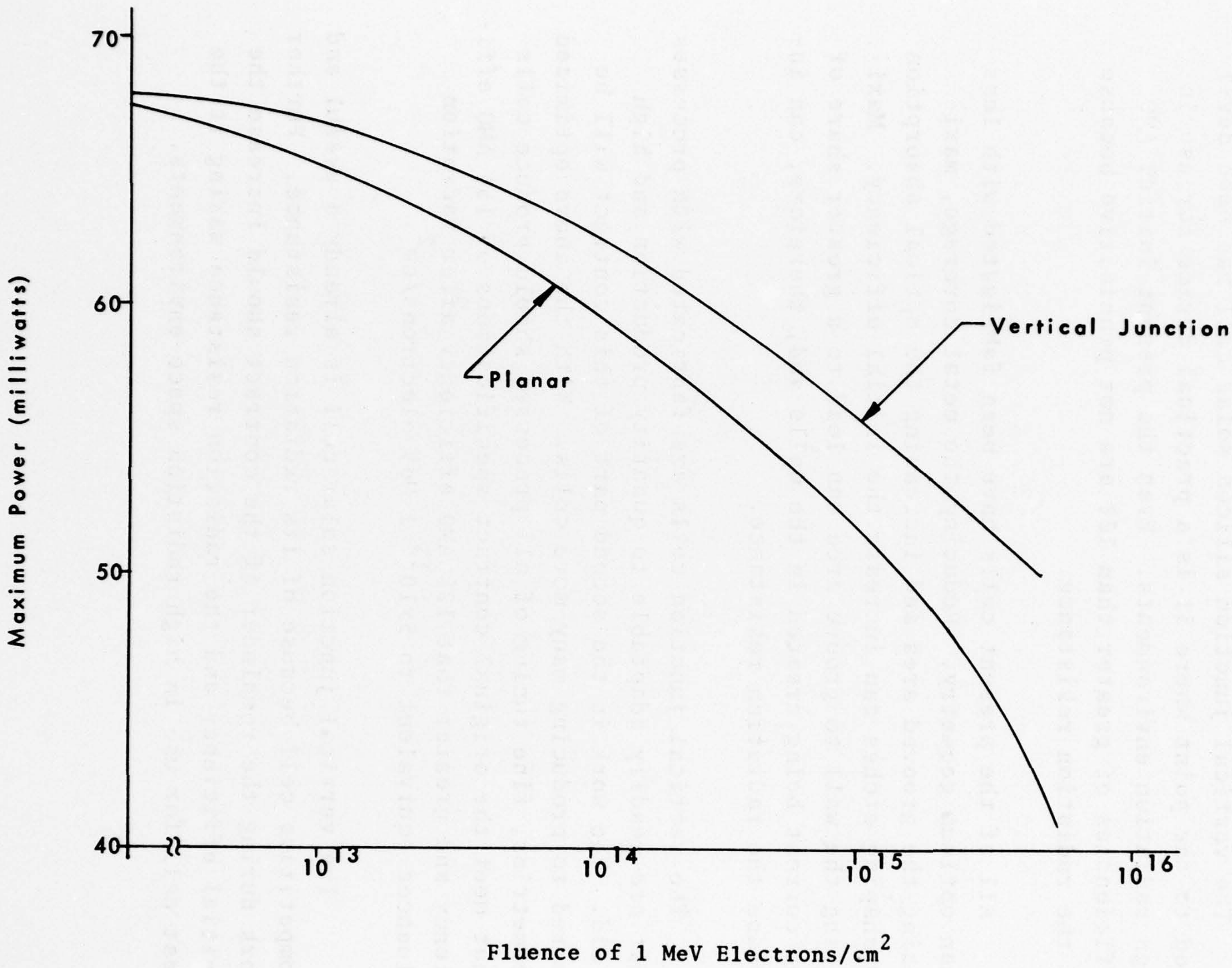

Figure 22: Radiation Degradation of the Maximum Power for Vertical Junction and Planar Silicon Solar Cells.

V. CONCLUSIONS

The vertical junction silicon solar cell has been developed to the point where it is a practical device for use in high radiation environments. Even the present initial AMO efficiencies of greater than 13% are not prohibitive because of the radiation resistance.

All of the present cells have been fabricated with less than optimum geometry. Reducing the metal coverage, maximizing the grooved area and increasing the optical absorption by shaping etches can increase the initial efficiency. Maximizing the wall to groove area can lead to a greater share of the current being created in the walls and, therefore, can increase the radiation resistance.

The vertical junction cells are fabricated with processes that are readily adaptable to quantity production and high yield. The work in the second part of this contract will be geared to producing many more cells. With the above optimized geometries, fine tuning of all processes should produce cells that meet the original contract specifications of 15% AMO efficiency and greater that 12% AMO efficiency after radiation fluences equivalent to 5×10^{15} 1 MeV electrons/cm^2.

The vertical junction solar cell is already a useful and competitive cell because of its radiation resistance. Further work during the remainder of the contract should increase the initial efficiency and the radiation resistance making it the best cell for use in high radiation space environments.

APPENDIX A

In order to determine the current generated by the incident light, one must find the currents generated by the photons in each wavelength range present in the incident sunlight and then sum the components. Each wavelength range can be given a specific absorption coefficient and photon flux. The absorption coefficients were taken from the work of Dash and Newman (Ref. 11) Figure A-1, and Phillip and Ehrenreich (Ref. 12) Figure A-2. The photon flux was taken from Thekaekara (Ref. 10). Both sets of values are tabulated in Table A-1. The carrier generation is calculated as a function of penetration distance into the silicon as tabulated in Table A-2 for the incremental change and in Table A-3 for the total carrier generation. The program calculated the carrier generation for wavelength bands of .01 microns and then summed the results into the .1 micron bands shown in the tables. Figure A-3 shows the absorption for each band and the total absorption. This data is then used as described in Section III.

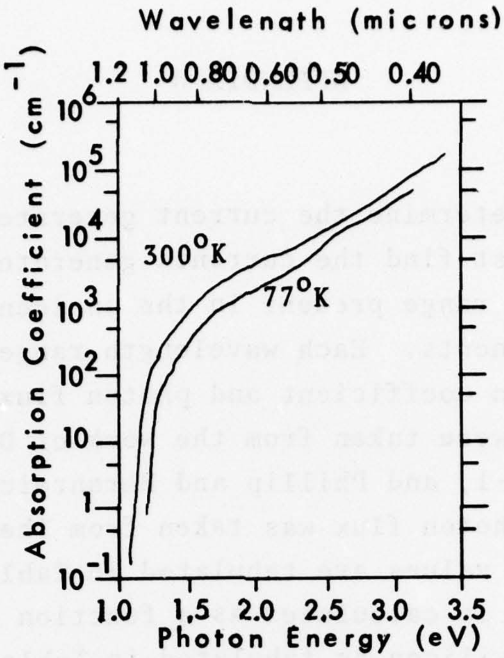

Figure A-1: Absorption Coefficient for Light in Silicon 1.2μ to 0.4μ Wavelength.

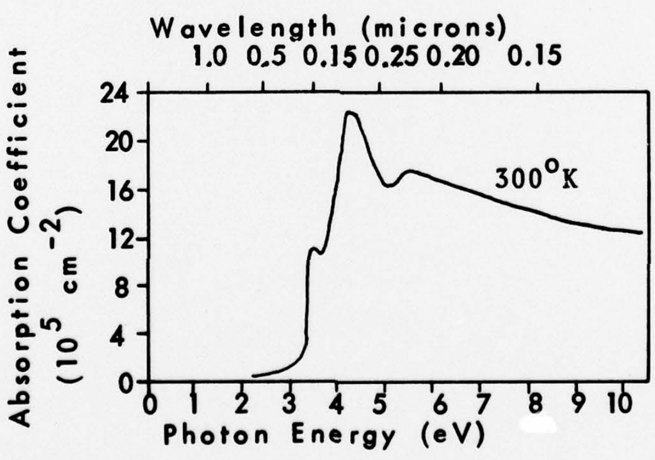

Figure A-2: Absorption Coefficient for Light to Silicon .5μ to 0.5μ Wavelength.

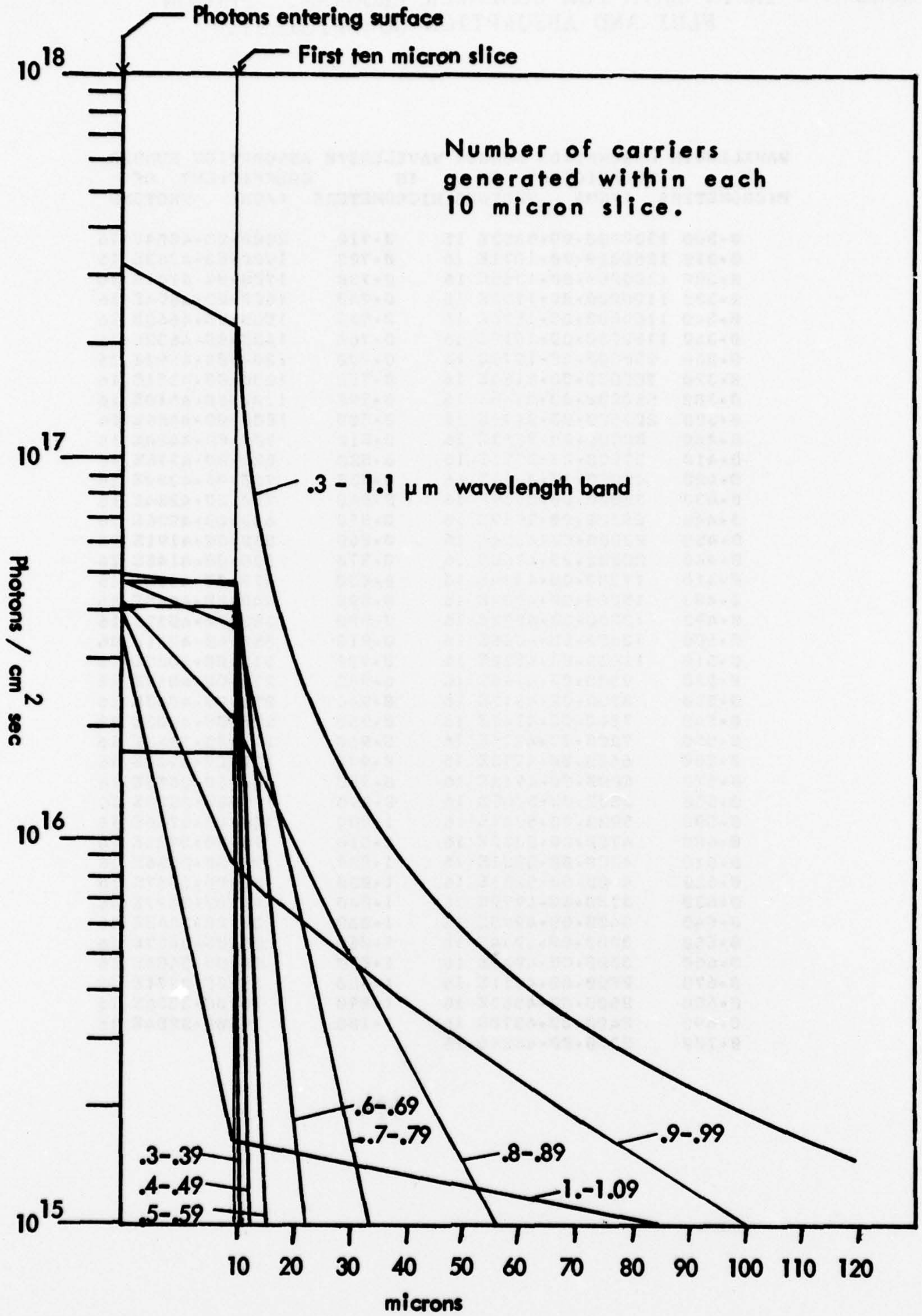

Figure A-3: Number of Carrier Pairs Generated Within Each 10 Micron Slice.

TABLE A-1 INPUT DATA FOR COMPUTER PROGRAM. PHOTON FLUX AND ABSORPTION COEFFICIENT.

WAVELENGTH IN MICROMETERS	ABSORPTION COEFFICIENT (/CM)	NUMBER OF PHOTONS	WAVELENGTH IN MICROMETERS	ABSORPTION COEFFICIENT (/CM)	NUMBER OF PHOTONS
0.300	1300000.00	.8352E 15	0.710	2800.00	.4804E 16
0.310	1250000.00	.1071E 16	0.720	1900.00	.4763E 16
0.320	1200000.00	.1368E 16	0.730	1700.00	.4741E 16
0.330	1100000.00	.1733E 16	0.740	1600.00	.4694E 16
0.340	1100000.00	.1830E 16	0.750	1500.00	.4663E 16
0.350	1100000.00	.1910E 16	0.760	1400.00	.4633E 16
0.360	950000.00	.1973E 16	0.770	1300.00	.4593E 16
0.370	700000.00	.2164E 16	0.780	1200.00	.4551E 16
0.380	500000.00	.2148E 16	0.790	1100.00	.4510E 16
0.390	200000.00	.2199E 16	0.800	1000.00	.4466E 16
0.400	80000.00	.2863E 16	0.810	900.00	.4424E 16
0.410	57000.00	.3371E 16	0.820	820.00	.4376E 16
0.420	42000.00	.3679E 16	0.830	760.00	.4329E 16
0.430	33000.00	.3559E 16	0.840	700.00	.4284E 16
0.440	28000.00	.3969E 16	0.850	640.00	.4236E 16
0.450	23000.00	.4524E 16	0.860	580.00	.4191E 16
0.460	20000.00	.4768E 16	0.870	530.00	.4148E 16
0.470	17000.00	.4824E 16	0.880	470.00	.4102E 16
0.480	15000.00	.4934E 16	0.890	440.00	.4068E 16
0.490	13000.00	.4832E 16	0.900	380.00	.4037E 16
0.500	12000.00	.4886E 16	0.910	350.00	.4031E 16
0.510	11000.00	.4832E 16	0.920	310.00	.4025E 16
0.520	9500.00	.4796E 16	0.930	270.00	.4017E 16
0.530	8700.00	.4915E 16	0.940	250.00	.4008E 16
0.540	7800.00	.4847E 16	0.950	220.00	.4003E 16
0.550	7200.00	.4776E 16	0.960	190.00	.3963E 16
0.560	6600.00	.4773E 16	0.970	170.00	.3921E 16
0.570	6000.00	.4913E 16	0.980	140.00	.3873E 16
0.580	5500.00	.5008E 16	0.990	120.00	.3823E 16
0.590	5200.00	.5049E 16	1.000	100.00	.3766E 16
0.600	4700.00	.5032E 16	1.010	90.00	.3702E 16
0.610	4300.00	.5021E 16	1.020	70.00	.3636E 16
0.620	4000.00	.5281E 16	1.030	55.00	.3567E 16
0.630	3700.00	.4979E 16	1.040	42.00	.3497E 16
0.640	3400.00	.4975E 16	1.050	30.00	.3468E 16
0.650	3200.00	.4944E 16	1.060	25.00	.3437E 16
0.660	3000.00	.4937E 16	1.070	20.00	.3404E 16
0.670	2800.00	.4911E 16	1.080	15.00	.3371E 16
0.680	2600.00	.4885E 16	1.090	10.00	.3336E 16
0.690	2400.00	.4870E 16	1.100	10.00	.3284E 16
0.700	2200.00	.4824E 16			

TABLE A-2 NUMBER OF CARRIER PAIRS GENERATED WITHIN EACH 10 MICRON SLICE.

DISTANCE INTO CELL IN MICRONS	WAVELENGTH BAND IN MICRONS .3-.39	WAVELENGTH BAND IN MICRONS .4-.49	WAVELENGTH BAND IN MICRONS .5-.59	WAVELENGTH BAND IN MICRONS .6-.69
	0.17236E 17	0.41575E 17	0.48802E 17	0.49836E 17
10	0.17236E 17	0.41575E 17	0.48728E 17	0.47786E 17
20	0.0	0.12642E 11	0.73558E 14	0.19330E 16
30	0.0	0.25157E 05	0.27869E 12	0.10934E 15
40	0.0	0.0	0.12724E 10	0.73964E 13
50	0.0	0.0	0.62449E 07	0.55110E 12
60	0.0	0.0	0.31021E 05	0.43491E 11
70	0.0	0.0	0.16332E 03	0.35619E 10
80	0.0	0.0	0.0	0.29919E 09
90	0.0	0.0	0.0	0.25585E 08
100	0.0	0.0	0.0	0.22168E 07
110	0.0	0.0	0.0	0.19397E 06
120	0.6	0.0	0.0	0.17099E 05
130	0.0	0.0	0.0	0.15147E 04
140	0.0	0.0	0.0	0.13390E 03
150	0.0	0.0	0.0	0.11323E 02
160	0.0	0.0	0.0	0.16212E-04
170	0.0	0.0	0.0	0.0
180	0.0	0.0	0.0	0.0
190	0.0	0.0	0.0	0.0
200	0.0	0.0	0.0	0.0
210	0.0	0.0	0.0	0.0
220	0.0	0.0	0.0	0.0
230	0.0	0.0	0.0	0.0
240	0.0	0.0	0.0	0.0
250	0.0	0.0	0.0	0.0

Total number of photons

0.32502E 18

	.7-.79	.8-.89	.9-.99	1.0-1.09		Whole Spectrum .3-1.10
	0.46776E 17	0.42624E 17	0.39701E 17	0.35183E 17		
10	0.36759E 17	0.26898E 17	0.84642E 16	0.15956E 16	10	0.22301E 18
20	0.76467E 16	0.10320E 17	0.64566E 16	0.14938E 16	20	0.27956E 17
30	0.17641E 16	0.52546E 16	0.49937E 16	0.13997E 16	30	0.13554E 17
40	0.44224E 15	0.27537E 16	0.38882E 16	0.13126E 16	40	0.84359E 16
50	0.11804E 15	0.14817E 16	0.30478E 16	0.12321E 16	50	0.59116E 16
60	0.32998E 14	0.81628E 15	0.24047E 16	0.11575E 16	60	0.44427E 16
70	0.95452E 13	0.45964E 15	0.19097E 16	0.10884E 16	70	0.34974E 16
80	0.28327E 13	0.26274E 15	0.15260E 16	0.10243E 16	80	0.28464E 16
90	0.85733E 12	0.15267E 15	0.12268E 16	0.96492E 15	90	0.23754E 16
100	0.26348E 12	0.89845E 14	0.99201E 15	0.90975E 15	100	0.20217E 16
110	0.81970E 11	0.53445E 14	0.80659E 15	0.85850E 15	110	0.17482E 16
120	0.25753E 11	0.32081E 14	0.65928E 15	0.81085E 15	120	0.15315E 16
130	0.81566E 10	0.19485E 14	0.54155E 15	0.76655E 15	130	0.13565E 16
140	0.26006E 10	0.11815E 14	0.44691E 15	0.72531E 15	140	0.12127E 16
150	0.83381E 09	0.72335E 13	0.37043E 15	0.68689E 15	150	0.10930E 16
160	0.26859E 09	0.44499E 13	0.30829E 15	0.65108E 15	160	0.99194E 15
170	0.86870E 08	0.27488E 13	0.25755E 15	0.61768E 15	170	0.90581E 15
180	0.28191E 08	0.17041E 13	0.21592E 15	0.58650E 15	180	0.83170E 15
190	0.91759E 07	0.10597E 13	0.18162E 15	0.55738E 15	190	0.76734E 15
200	0.29942E 07	0.66084E 12	0.15324E 15	0.53014E 15	200	0.71106E 15
210	0.97922E 06	0.41309E 12	0.12965E 15	0.50467E 15	210	0.66149E 15
220	0.32087E 06	0.25879E 12	0.10999E 15	0.48082E 15	220	0.61755E 15
230	0.10532E 06	0.16243E 12	0.93538E 14	0.45847E 15	230	0.57840E 15
240	0.34622E 05	0.10213E 12	0.79726E 14	0.43751E 15	240	0.54329E 15
250	0.11396E 05	0.64310E 11	0.66098E 14	0.41784E 15	250	0.51171E 15

TABLE A-3 TOTAL NUMBER OF CARRIER PAIRS GENERATED BETWEEN THE FRONT SURFACE AND THE SPECIFIED DISTANCE.

TOTAL NUMBER OF CARRIERS GENERATED BETWEEN FRONT AND THIS MANY MICRONS (Thickness) — Wavelength Band

Thickness (MICRONS)	.3-.39	.4-.49	.5-.59	.6-.69
10	0.17236E 17	0.41575E 17	0.48728E 17	0.47786E 17
20	0.17236E 17	0.41575E 17	0.48802E 17	0.49719E 17
30	0.17236E 17	0.41575E 17	0.48802E 17	0.49828E 17
40	0.17236E 17	0.41575E 17	0.48802E 17	0.49835E 17
50	0.17236E 17	0.41575E 17	0.48802E 17	0.49836E 17
60	0.17236E 17	0.41575E 17	0.48802E 17	0.49836E 17
70	0.17236E 17	0.41575E 17	0.48802E 17	0.49836E 17
80	0.17236E 17	0.41575E 17	0.48802E 17	0.49836E 17
90	0.17236E 17	0.41575E 17	0.48802E 17	0.49836E 17
100	0.17236E 17	0.41575E 17	0.48802E 17	0.49836E 17
110	0.17236E 17	0.41575E 17	0.48802E 17	0.49836E 17
120	0.17236E 17	0.41575E 17	0.48802E 17	0.49836E 17
130	0.17236E 17	0.41575E 17	0.48802E 17	0.49836E 17
140	0.17236E 17	0.41575E 17	0.48802E 17	0.49836E 17
150	0.17236E 17	0.41575E 17	0.48802E 17	0.49836E 17
160	0.17236E 17	0.41575E 17	0.48802E 17	0.49836E 17
170	0.17236E 17	0.41575E 17	0.48802E 17	0.49836E 17
180	0.17236E 17	0.41575E 17	0.48802E 17	0.49836E 17
190	0.17236E 17	0.41575E 17	0.48802E 17	0.49836E 17
200	0.17236E 17	0.41575E 17	0.48802E 17	0.49836E 17
210	0.17236E 17	0.41575E 17	0.48802E 17	0.49836E 17
220	0.17236E 17	0.41575E 17	0.48802E 17	0.49836E 17
230	0.17236E 17	0.41575E 17	0.48802E 17	0.49836E 17
240	0.17236E 17	0.41575E 17	0.48802E 17	0.49836E 17
250	0.17236E 17	0.41575E 17	0.48802E 17	0.49836E 17

Thickness (MICRONS)	.7-.79	.8-.89	.9-.99	1.0-1.90		Whole Spectrum .3-1.10
10	0.36759E 17	0.28898E 17	0.84042E 16	0.15956E 16	10	0.22301E 18
20	0.44405E 17	0.31218E 17	0.14861E 17	0.30894E 16	20	0.25097E 18
30	0.46169E 17	0.36473E 17	0.19854E 17	0.44891E 16	30	0.26452E 18
40	0.46612E 17	0.39226E 17	0.23743E 17	0.58017E 16	40	0.27296E 18
50	0.46730E 17	0.40708E 17	0.26790E 17	0.70338E 16	50	0.27887E 18
60	0.46763E 17	0.41524E 17	0.29195E 17	0.81914E 16	60	0.28331E 18
70	0.46772E 17	0.41983E 17	0.31105E 17	0.92798E 16	70	0.28681E 18
80	0.46775E 17	0.42246E 17	0.32631E 17	0.10304E 17	80	0.28966E 18
90	0.46776E 17	0.42399E 17	0.33858E 17	0.11269E 17	90	0.29203E 18
100	0.46776E 17	0.42489E 17	0.34850E 17	0.12179E 17	100	0.29405E 18
110	0.46776E 17	0.42542E 17	0.35656E 17	0.13037E 17	110	0.29580E 18
120	0.46776E 17	0.42574E 17	0.36315E 17	0.13848E 17	120	0.29733E 18
130	0.46776E 17	0.42594E 17	0.36857E 17	0.14615E 17	130	0.29869E 18
140	0.46776E 17	0.42605E 17	0.37304E 17	0.15340E 17	140	0.29990E 18
150	0.46776E 17	0.42613E 17	0.37674E 17	0.16027E 17	150	0.30100E 18
160	0.46776E 17	0.42617E 17	0.37983E 17	0.16678E 17	160	0.30199E 18
170	0.46776E 17	0.42620E 17	0.38240E 17	0.17296E 17	170	0.30289E 18
180	0.46776E 17	0.42622E 17	0.38456E 17	0.17882E 17	180	0.30373E 18
190	0.46776E 17	0.42623E 17	0.38638E 17	0.18440E 17	190	0.30449E 18
200	0.46776E 17	0.42623E 17	0.38791E 17	0.18970E 17	200	0.30520E 18
210	0.46776E 17	0.42624E 17	0.38921E 17	0.19474E 17	210	0.30587E 18
220	0.46776E 17	0.42624E 17	0.39031E 17	0.19955E 17	220	0.30648E 18
230	0.46776E 17	0.42624E 17	0.39124E 17	0.20414E 17	230	0.30706E 18
240	0.46776E 17	0.42624E 17	0.39204E 17	0.20851E 17	240	0.30761E 18
250	0.46776E 17	0.42624E 17	0.39272E 17	0.21269E 17	250	0.30812E 18

REFERENCES

(1) Wise, J. F.: Vertical Junction Solar Cell, U.S. Patent 3,690,953.

(2) Rahilly, W. P.: Vertical Multijunction Solar Cells. Conference Record of the Ninth IEEE Photovoltaic Specialists Conference, May 1972, pp. 44-52.

(3) Stella, P. and Gover, A.: Vertical Multijunction Solar Cell. Conference Record of the Ninth IEEE Photovoltaic Conference, May 1972, p. 85.

(4) Chadd, T. B. S., and Wolf, M.: The Effect of Surface Recombination Velocity on the Performance of Vertical Junction Solar Cells. Conference Record of the Ninth IEEE Photovoltaic Specialists Conference, May 1972, p. 87.

(5) Smeltzer, R. K., Hotz, R., and Shah, P.: Development of Vertical Multijunction Solar Cells for Spacecraft Primary Power. Technical Report AFAPL - TR-74-45, June 1974.

(6) Lloyd, W. W., Yeakley, R., Fuller, C., and Malone, F.: Development of Vertical Multijunction Solar Cells for Spacecraft Primary Power. Technical Report AFAPL - TR-74-45, Vol. II, June 1975.

(7) Lloyd, W. W.: Fabrication of an Improved Multijunction Solar Cell. Conference Record of the Eleventh IEEE Photovoltaic Specialists Conference, 1975, p. 349.

(8) Mendel, M., and Yang, K.: Polishing of Silicon by the Cupric Ion Process. Proceedings of the IEEE, 50, Sept. 1969, pp. 1476-1480.

(9) Kendall, D. L.: On Etching Very Narrow Grooves in Silicon. Applied Physics Letters, 26, February, 1975, pp. 195-198.

(10) Thekaekara, M. P.: Extra-Terrestrial Solar Energy and Its Possible Variations. International Congress, Photovoltaic Section, Paris, July 1973.

(11) Dash, W. C., and Newman, R.: Intrinsic Optical Absorption in Single Crystal Germanium and Silicon at 77° and 300°K. Phys. Rev. 99, August 1955, pp. 1151-1156.

(12) Phillip, H. R., and Ehrenreich, H.: Optical Constants of Silicon in the Region 1 to 10 eV. Phys. Rev., 120, October 1960, pp. 37-38.

(13) Lindmayer, J., et al: Development of 20% Efficient Solar Cell: Final Report for NSF Grant GI-43090, pp. 87, October 1975.

(14) Larin, F.: Radiation Effects in Semiconductor Devices, p. 211, from a graph summarizing the work of R. G. Downing (1968).

(15) Larin, F.: Ibid., p. 215, in summarizing the work of J. R. Belinski et al (1968).

(16) Srour, J. R., Othmer, S., and Chiu, K. Y.: Electron and Proton Damage Coefficients in Low-Resistivity Silicon. IEEE Trans. Nucl. Sci. NS 22, 2656 (December 1969).

(17) Stofel, E. J., Stewart, T. B., and Ornelas, J. R.: Neutron Damage to Silicon Solar Cells. IEEE Trans. Nucl. Sci. NS-16, No. 5 (October 1969).

(18) Brucker, G. J., and Markow, B.: Neutron Damage in Silicon Solar Cells: Conference Record of the Sixth Photovoltaic Specialists Conference, Cocoa Beach, Fla. (March 1967).

☆U.S.Government Printing Office: 1977 — 757-001/11

AFAPL/ POE-2
WRIGHT-PATTERSON AFB OH 45433

UNITED STATES AIR FORCE
OFFICIAL BUSINESS